Japanese Journal of Applied Physics
Vol. 45, No. 10A, 2006, pp. 8005–8009

Enhanced Magnification Angiography Using 20-μm-Focus Tungsten Tube

Toshiyuki ENOMOTO, Eiichi SATO[1], Yoshinobu SUMIYAMA, Katsuo AIZAWA[2], Manabu WATANABE, Etsuro TANAKA[3], Hidezo MORI[4], Hiroki KAWAKAMI[5], Toshiaki KAWAI[5], Takashi INOUE[6], Akira OGAWA[6] and Shigehiro SATO[7]

The 3rd Department of Surgery, Toho University School of Medicine, 2-17-6 Ohashi, Meguro-ku, Tokyo 153-8515, Japan
[1]*Department of Physics, Iwate Medical University, 3-16-1 Honchodori, Morioka 020-0015, Japan*
[2]*Tokyo Medical University [emeritus professor], 6-1-1 Shinjuku, Shinjuku-ku, Tokyo 160-8402, Japan*
[3]*Department of Nutritional Science, Faculty of Applied Bio-science, Tokyo University of Agriculture, 1-1-1 Sakuragaoka, Setagaya-ku, Tokyo 156-8502, Japan*
[4]*Department of Cardiac Physiology, National Cardiovascular Center Research Institute, 5-7-1 Fujishirodai, Suita, Osaka 565-8565, Japan*
[5]*Electron Tube Division #2, Hamamatsu Photonics K.K., 314-5 Shimokanzo, Iwata, Shizuoka 438-0193, Japan*
[6]*Department of Neurosurgery, School of Medicine, Iwate Medical University, 19-1 Uchimaru, Morioka 020-8505, Japan*
[7]*Department of Microbiology, School of Medicine, Iwate Medical University, 19-1 Uchimaru, Morioka 020-8505, Japan*

(Received April 10, 2006; accepted June 25, 2006; published online October 6, 2006)

A microfocus X-ray tube is useful for performing magnification radiography, and its X-ray generator (L9631, Hamamatsu Photonics) consists of a personal computer for controlling the tube voltage and current, and a main unit with a high-voltage circuit and a fixed-anode X-ray tube. The maximum tube voltage, current, and electric power were 110 kV, 800 μA, and 50 W, respectively. The focal-spot size was proportional to the electric power of the tube, and the size was approximately 20 μm with a power of 20 W. Using a 3-mm-thick aluminum filter, the X-ray intensity was 7.75 μGy/s at 1.0 m from the source with a tube voltage of 60 kV and a current of 100 μA. Because the peak photon energy was approximately 38 keV using the filter with a tube voltage of 60 kV, the bremsstrahlung X-rays were absorbed effectively by iodine-based contrast media at an iodine K-edge of 33.2 keV. Enhanced angiography was performed by fourfold magnification imaging with a computed radiography system using iodine-based microspheres 15 μm in diameter. In the angiography of nonliving animals, we observed fine blood vessels of approximately 100 μm with high contrast. [DOI: 10.1143/JJAP.45.8005]

KEYWORDS: high-contrast angiography, magnification digital radiography, microfocus X-ray tube, energy-selective imaging

1. Introduction

To perform high-speed medical radiography, several various flash X-ray generators using cold-cathode tubes have been developed.[1–4] In particular, quasi-monochromatic flash X-ray generators[5–10] have been designed to perform preliminary experiments for producing clean K-series X-rays, and higher-harmonic hard X-rays have been observed in a weakly ionized linear plasma of copper and nickel. However, in monochromatic flash radiography, difficulties in increasing X-ray duration and in performing X-ray computed tomography (CT) have been encountered.

Synchrotrons are capable of producing high-dose-rate monochromatic parallel X-ray beams using silicon crystals, and the beams have been applied to phase-contrast radiography[11,12] and enhanced K-edge angiography.[13,14] In angiography, monochromatic X-rays with photon energies ranging from 33.3 to 35 keV have been employed because the rays are absorbed effectively by iodine-based contrast media with an iodine K-edge of 33.2 keV.

Without using synchrotrons, phase-contrast radiography[15] for edge enhancement can be performed using a microfocus X-ray tube, and the enhancement has been achieved in mammography[16] with a computed radiography (CR) system[17] using a 100-μm-focus tube. Subsequently, we developed a cerium X-ray generator[18,19] to perform enhanced K-edge angiography using cone beams, and succeeded in observing fine blood vessels and coronary arteries with high contrast using cerium Kα-rays of 34.6 keV.

Although the magnification radiography is used to improve the spatial resolution in angiography utilizing a digital imaging system, it is difficult to design a small focus cerium tube for angiography. Therefore, narrow-photon-energy bremsstrahlung X-rays[20–22] with a peak energy of approximately 35 keV from a tungsten tube are used to perform high-contrast angiography.

In this research, we employed a microfocus tungsten tube, and performed enhanced magnification angiography by controlling bremsstrahlung X-ray spectra using an aluminum filter.

2. Principle of Enhanced Magnification Angiography

Figure 1 shows the mass attenuation coefficients of iodine at the selected energies; the coefficient curve is discontinuous at the iodine K-absorption edge of 33.2 keV. The effective bremsstrahlung X-rays for K-edge angiography are shown above the K-edge. Using a 3.0-mm-thick aluminum filter for absorbing soft X-rays, the peak photon energy of the bremsstrahlung rays increases to approximately 38 keV. In angiography, iodine contrast media in blood vessels easily absorb the rays, and soft bremsstrahlung rays are absorbed effectively by objects (muscles). Therefore, blood vessels are observed with high contrast. Subsequently, spatial resolution is improved by fourfold magnification imaging using a microfocus X-ray tube in conjunction with a CR system (Regius 150, Konica Minolta) at a sampling pitch of 87.5 μm.

3. Experimental Methods

The microfocus X-ray generator (L9631, Hamamatsu Photonics) consists of a personal computer and a system unit. The unit includes all the hardware in the X-ray generator, such as, a high-voltage circuit and a fixed anode X-ray tube. Tube voltage, current, and exposure time can be controlled by the computer. The maximum tube voltage, current, and electric power were 110 kV, 800 μA, and 50 W,

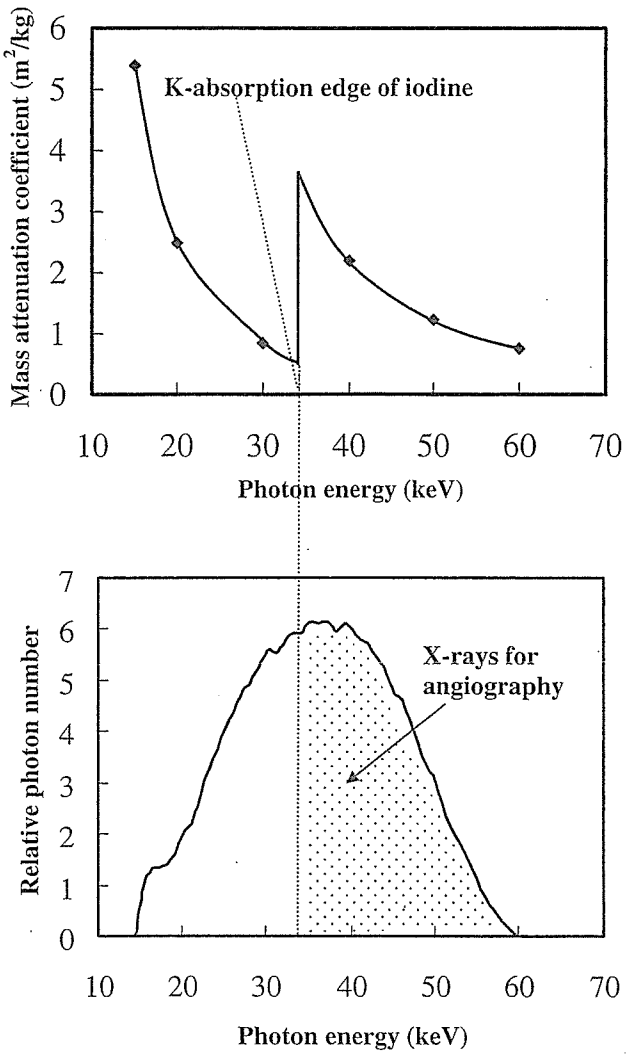

Fig. 1. Mass attenuation coefficients of iodine and bremsstrahlung X-rays for enhanced K-edge angiography.

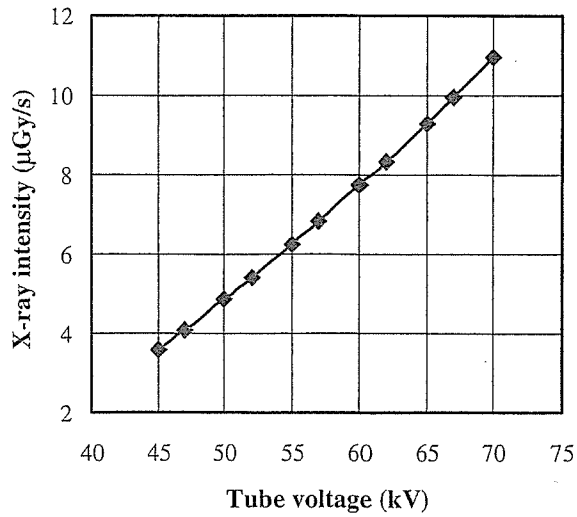

Fig. 2. X-ray intensity (μGy/s) as a function of tube voltage (kV) with tube current of 100 μA.

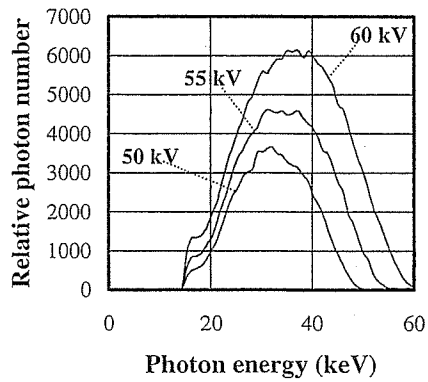

Fig. 3. Bremsstrahlung X-ray spectra measured using cadmium telluride detector with changes in tube voltage.

respectively. The focal-spot size was proportional to the electric power of the tube, and its size was approximately 20 μm in diameter with a power of 20 W. In this experiment, the tube voltage applied ranged from 45 to 70 kV, and the tube current was regulated to within 170 μA. The exposure time is controlled to obtain optimum X-ray intensity for angiography, and narrow-photon-energy bremsstrahlung X-rays are produced using the aluminum filter.

4. Results

4.1 X-ray intensity

X-ray intensity was measured using a Victoreen 660 ionization chamber, with a volume of 400 cm^3, at 1.0 m from the X-ray source using the filter (Fig. 2). At a constant tube current of 100 μA, X-ray intensity increased when tube voltage was increased. At a tube voltage of 60 kV, the X-ray intensity with the filter was 7.75 μGy/s.

4.2 X-ray spectra

To measure X-ray spectra using the filter, we employed a cadmium telluride detector (CDTE2020X, Hamamatsu Photonics) (Fig. 3). When tube voltage was increased, bremsstrahlung X-ray intensity increased, and both maximum photon energy and spectrum peak energy increased.

To perform K-edge angiography, bremsstrahlung X-rays of approximately 35 keV are used; the high-energy bremsstrahlung X-rays decrease image contrast. When this filter was used, because bremsstrahlung X-rays with energies higher than 60 keV were not absorbed easily, the tube voltage for angiography was determined to be 60 kV by considering the filtering effect of radiographic objects.

4.3 Enhanced magnification angiography

The enhanced angiography was performed by fourfold magnification imaging using the CR system and the filter at a tube voltage of 60 kV, and the distance between the X-ray source and the imaging plate was 1.0 m (Fig. 4). First, the spatial resolutions of cohesion and magnification radiographies were realized using a lead test chart at an exposure time of 30 s. In the magnification radiography, 50-μm-thick lines (10 line pairs) were clearly visible (Fig. 5). Figure 6 shows radiograms of tungsten wires in a 25-mm-diameter rod made of poly(methyl methacrylate) (PMMA) at an exposure time of 30 s. Although image contrast decreased slightly with decreasing wire diameter owing to the blurring of the image caused by the sampling pitch of 87.5 μm, a 20-μm-diameter wire could be observed.

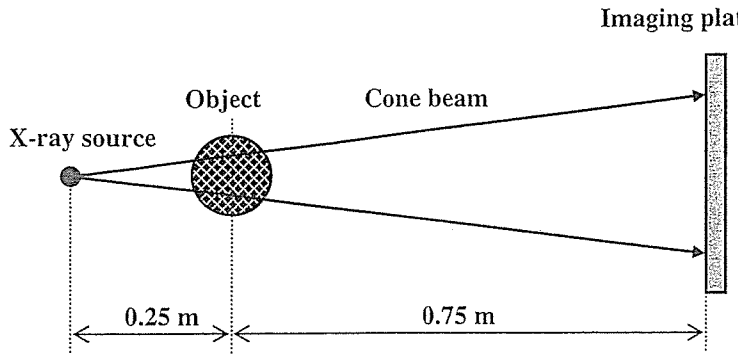

Fig. 4. Fourfold magnification imaging using imaging plate in conjunction with microfocus tube.

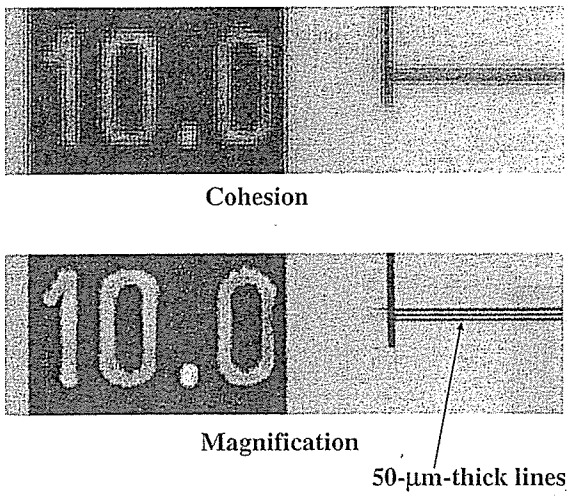

Fig. 5. Radiogram of test chart for measuring spatial resolution.

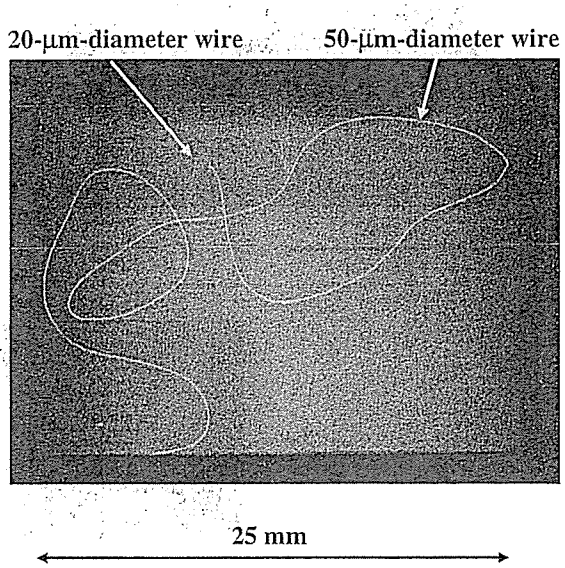

Fig. 6. Radiograms of tungsten wires in PMMA rod.

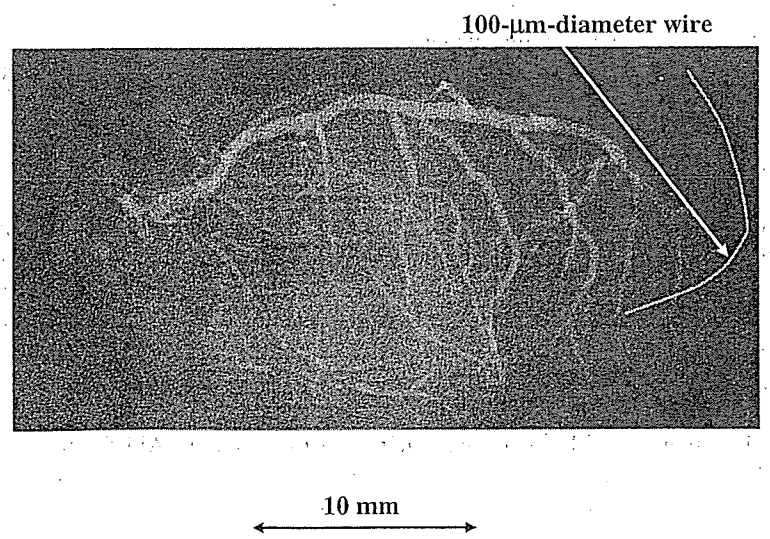

Fig. 7. Angiogram of extracted rabbit heart using iodine microspheres.

Figures 7 and 8 show angiograms of a 19-mm-thick rabbit heart specimen and a 41-mm-thick thigh specimen, respectively. The exposure time was 30 s, and these images were obtained using iodine microspheres of 15 μm diameter. The microspheres are very useful for making the phantoms of nonliving animals used for angiography. The iodine plastic spheres contained 37% iodine by weight, and the coronary arteries and fine blood vessels were visible.

Figure 9 shows angiograms of a dog heart specimen of 65 mm thickness using iodine spheres with an exposure time of 60 s. Although the image contrast decreased slightly with increasing thickness of the PMMA plate facing the X-ray

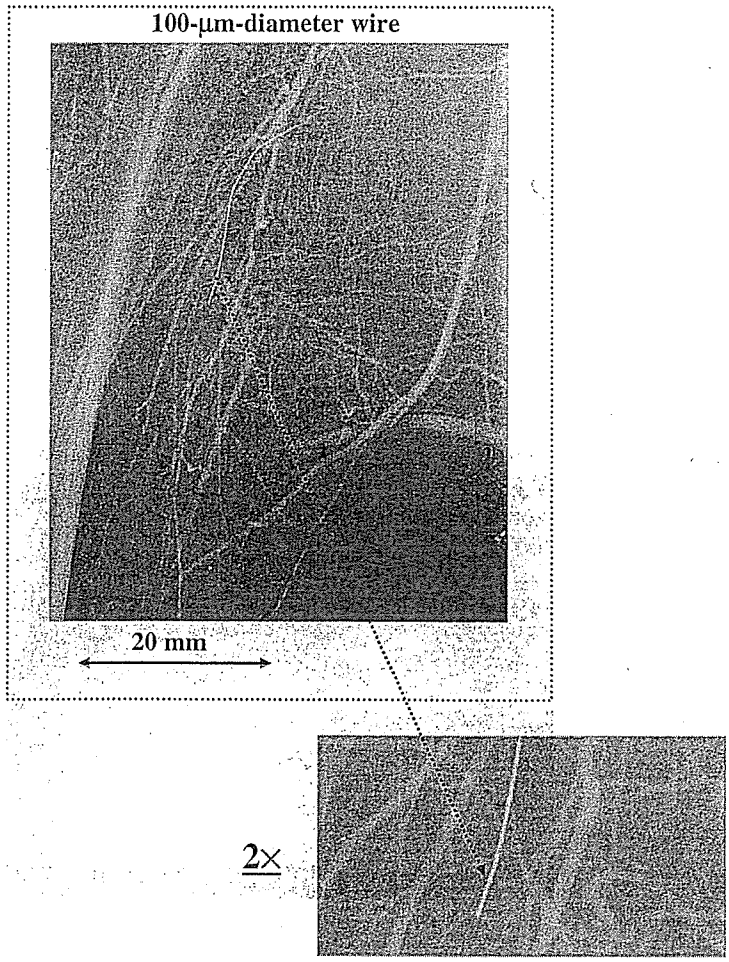

Fig. 8. Angiograms of rabbit thigh.

source, the coronary arteries of approximately 100 μm diameter were observed using a 100-mm-thick plate.

5. Conclusions

We employed a microfocus X-ray generator with a tungsten target tube to perform enhanced magnification angiography using narrow-photon-energy bremsstrahlung X-rays at a peak photon energy of approximately 38 keV, which can be absorbed easily by iodine-based contrast media. Although bremsstrahlung X-ray intensity substantially increased with increasing tube voltage, the optimal tube voltage for increasing image contrast was determined to be 60 kV.

Because the sampling pitch of the CR system is 87.5 μm, we obtained spatial resolutions of approximately 50 μm using fourfold magnification imaging achieved with a 20-μm-focus tube. To observe fine blood vessels of less than 100 μm diameter, the spatial resolution of the CR system should be improved to 43.8 μm (Regius 190, Konica Minolta), and iodine density should be increased.

In this research, we controlled bremsstrahlung X-rays to the optimum spectral distribution for realizing enhanced angiography using iodine-based contrast media. On the other hand, gadolinium-based contrast media with a K-edge energy of 50.2 keV have been employed to perform angiography in MRI, and the gadolinium density used has been increasing. In view of this situation, tungsten Kα rays (58.9 keV) are useful for enhancing K-edge angiography, because the Kα rays are absorbed effectively by gadolinium media. As compared with angiography using iodine media, the absorbed dose can be decreased considerably using gadolinium media.

At a tube voltage of 60 kV and a current of 170 μA, the photon number was approximately 2×10^7 photons/(cm^2·s) at 1.0 m from the source, and photon count rate can be increased easily using a rotating anode microfocus tube developed by Hitachi Medical Corporation. Recently, the maximum electric power of the microfocus X-ray tube has been increasing, and a kilowatt-range tube is realizable. Therefore, real-time magnification radiography will become possible using a flat panel detector with a pixel size of less than 100 μm.

Acknowledgments

This work was supported by Grants-in-Aid for Scientific Research (13470154, 13877114, and 16591222) and Advanced Medical Scientific Research from MECSST, Health and Labor Sciences Research Grants (RAMT-nano-001, RHGTEFB-genome-005 and RHGTEFB-saisei-003), and grants from the Keiryo Research Foundation, Promotion and Mutual Aid Corporation for Private Schools of Japan, Japan Science and Technology Agency (JST), and New Energy and Industrial Technology Development Organization (NEDO, Industrial Technology Research Grant Program in '03).

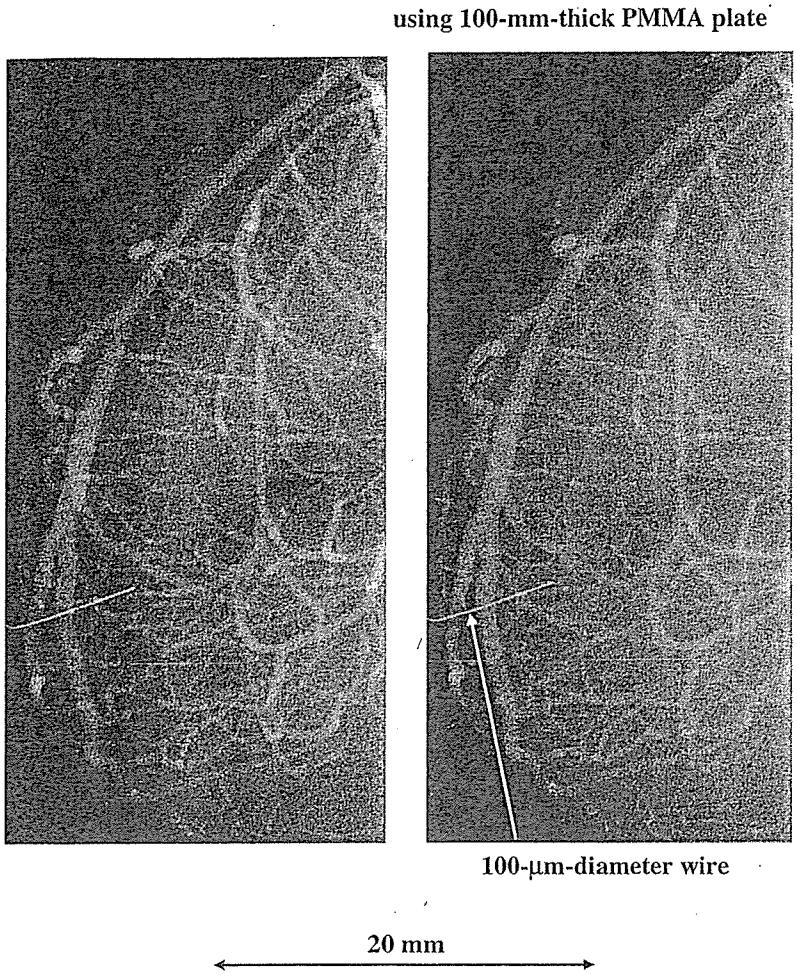

Fig. 9. Angiograms of extracted dog heart.

1) E. Sato, S. Kimura, S. Kawasaki, H. Isobe, K. Takahashi, Y. Tamakawa and T. Yanagisawa: Rev. Sci. Instrum. **61** (1990) 2343.
2) K. Takahashi, E. Sato, M. Sagae, T. Oizumi, Y. Tamakawa and T. Yanagisawa: Jpn. J. Appl. Phys. **33** (1994) 4146.
3) E. Sato, K. Takahashi, M. Sagae, S. Kimura, T. Oizumi, Y. Hayasi, Y. Tamakawa and T. Yanagisawa: Med. Biol. Eng. Comput. **32** (1994) 289.
4) E. Sato, M. Sagae, K. Takahashi, A. Shikoda, T. Oizumi, Y. Hayasi, Y. Tamakawa and T. Yanagisawa: Med. Biol. Eng. Comput. **32** (1994) 295.
5) E. Sato, Y. Hayasi, R. Germer, E. Tanaka, H. Mori, T. Kawai, T. Ichimaru, K. Takayama and H. Ido: Rev. Sci. Instrum. **74** (2003) 5236.
6) E. Sato, Y. Hayasi, R. Germer, E. Tanaka, H. Mori, T. Kawai, T. Ichimaru, S. Sato, K. Takayama and H. Ido: J. Electron Spectrosc. Relat. Phenom. **137–140** (2004) 713.
7) E. Sato, E. Tanaka, H. Mori, T. Kawai, S. Sato and K. Takayama: Opt. Eng. **44** (2005) 049002.
8) E. Sato, M. Sagae, E. Tanaka, Y. Hayasi, R. Germer, H. Mori, T. Kawai, T. Ichimaru, S. Sato, K. Takayama and H. Ido: Jpn. J. Appl. Phys. **43** (2004) 7324.
9) E. Sato, E. Tanaka, H. Mori, T. Kawai, T. Ichimaru, S. Sato, K. Takayama and H. Ido: Med. Phys. **32** (2005) 49.
10) E. Sato, Y. Hayasi, K. Kimura, E. Tanaka, H. Mori, T. Kawai, T. Inoue, A. Ogawa, S. Sato, K. Takayama, J. Onagawa and H. Ido: Jpn. J. Appl. Phys. **44** (2005) 8716.
11) A. Momose, T. Takeda, Y. Itai and K. Hirano: Nat. Med. **2** (1996) 473.
12) M. Ando, A. Maksimenko, H. Sugiyama, W. Pattanasiriwisawa, K. Hyodo and C. Uyama: Jpn. J. Appl. Phys. **41** (2002) L1016.
13) H. Mori, K. Hyodo, E. Tanaka, M. U. Mohammed, A. Yamakawa, Y. Shinozaki, H. Nakazawa, Y. Tanaka, T. Sekka, Y. Iwata, S. Honda, K. Umetani, H. Ueki, T. Yokoyama, K. Tanioka, M. Kubota, H. Hosaka, N. Ishizawa and M. Ando: Radiology **201** (1996) 173.
14) K. Hyodo, M. Ando, Y. Oku, S. Yamamoto, T. Takeda, Y. Itai, S. Ohtsuka, Y. Sugishita and J. Tada: J. Synchrotron Radiat. **5** (1998) 1123.
15) S. W. Wilkins, T. E. Gureyev, D. Gao, A. Pogany and A. W. Stevenson: Nature **384** (1996) 335.
16) A. Ishisaka, H. Ohara and C. Honda: Opt. Rev. **7** (2000) 566.
17) E. Sato, K. Sato and Y. Tamakawa: Annu. Rep. Iwate Med. Univ. School Liberal Arts Sci. **35** (2000) 13.
18) E. Sato, E. Tanaka, H. Mori, T. Kawai, T. Ichimaru, S. Sato, K. Takayama and H. Ido: Med. Phys. **31** (2004) 3017.
19) E. Sato, E. Tanaka, H. Mori, T. Kawai, T. Inoue, A. Ogawa, A. Yamadera, S. Sato, F. Ito, K. Takayama, J. Onagawa and H. Ido: Jpn. J. Appl. Phys. **44** (2005) 8204.
20) A. B. Crummy, C. A. Mistretta, M. G. Ort, F. Kelcz, J. R. Cameron and M. P. Siedband: Radiology **8** (1973) 402.
21) R. A. Kruger, C. A. Mistretta, A. B. Crummy, J. F. Sackett, M. M. Goodsit, S. J. Riederer, T. L. Houk, C. G. Shaw and D. Flemming: Radiology **125** (1977) 234.
22) F. Kelcz and C. A. Mistretta: Med. Phys. **3** (1977) 159.

Tokai J Exp Clin Med., Vol. 31, No. 2, pp. 49-52, 2006

Efficient Preparation of Cationized Gelatin for Gene Transduction

Naoto FUKUYAMA, Tsuyoshi ONUMA[*1], Shio JUJO, Yoshifumi TAMAI[*2], Takahiro SUZUKI[*3], Kazunori MYOJIN[*4], Yasuhiko TABATA[*5], Yoshimi ISHIHARA[*1], Jiro TAKANO[*1] and Hidezo MORI[*6]

*Department of Physiology, [*2] Department of Radiation Oncology,*
*[*3] Department of Ophthalmology, [*4] Department of Radiology, Tokai University School of Science*
*[*1] Department of Chemistry, Tokai University School of Science*
*[*5] Department of Frontier Medical Sciences, Kyoto University*
*[*6] Department of Cardiac Physiology, National Cardiovascular Center*

(Received November 21, 2005; Accepted April 12, 2006)

We previously reported gene therapy using cationized gelatin microspheres of ϕ20-32 μm, prepared from pig skin, as a transducing agent, but although the gelatin offered various advantages, its yield was extremely low (only 0.1%). In this study, we markedly improved the yield of ϕ20-32 μm cationized gelatin microspheres and prepared a newly less than ϕ20 μm cationized gelatin. Conventionally, cationized gelatin is prepared by cationization, particulation by agitation, and cross-linking. The yield is determined by the particulation step, for which we had used a three-necked distillation flask of 500 mL and an agitation speed of 420 rpm. The yield was significantly increased from 0.13 ± 0.02% to 8.80 ± 1.90% by using a smaller flask of 300 mL and an agitation speed of 25000 rpm ($p < 0.01$). We could also prepare cationized gelatin of less than ϕ20 μm, which had not been possible previously. We confirmed that efficient gene introduction into peritoneal macrophages could be achieved with the new cationized gelatin.

Key words: gelatine microsphere, macrophage, yield

INTRODUCTION

Efficient gene transduction methods are necessary for gene therapy [1], and currently available methods can be divided into viral vector techniques and non-viral approaches, such as lipofection or electroporation. Viral vectors such as adenovirus or retrovirus offer high transduction efficiency, but there are questions regarding safety [2]. On the other hand, the efficiency of transduction with non-viral vectors is generally poor [3]. In recent years, nucleofection has been developed for highly efficient gene transduction, but it can be applied to only certain cells, and it causes damage in some cases [4].

We showed that intramuscular injection of FGF-4 gene-gelatin complex induced significantly greater angiogenesis than injection of the bare FGF-4 gene [5]. Furthermore, we showed that adrenomedullin (AM) gene-gelatin complex effectively transduced the AM gene into endothelial progenitor cells (EPCs), and the transduced EPCs had a therapeutic effect in pulmonary hypertension [6]. In those studies, we used cationized gelatin microspheres of ϕ20-32 μm, derived from pig skin. However, the yield of gelatin was only about 0.1%. Cascone *et al.* reported that the preparation of nanoparticulate gelatin required an agitation speed of cationized gelatin and olive oil of more than 10,000 rpm [7], so in this study, we examined whether the use of a higher agitation speed during preparation of the gelatin particles would increase the yield and reduce the particle size in our procedure. We also confirmed the efficacy of the gelatin particles thus obtained for gene transduction.

MATERIALS

Gelatin of pig skin origin (PI 9) was purchased from Nitta Gelatin Corp, Japan. 1-Ethyl-3-(3-dimethylaminopropyl) carbodiimide (EDC), β-alanine, acetone, glycine, hydrochloric acid, ethylenediamine, olive oil, glutaraldehyde solution (GA), potassium dihydrogenphosphate, disodium hydrogenphosphate and sodium hydrogen carbonate were purchased from Wako Pure Chemical Industry, Japan. Liquid nitrogen was purchased from Tomoe Corporation, Japan.

Rat peritoneal macrophages were collected by intraperitoneal injection of thioglycolate culture medium as previously described [8]. DNA encoding GFP with the cytomegalovirus enhancer-chicken β-actin hybrid promoter was constructed [5].

METHODS

Conventional preparation of gelatin microspheres involves three steps: (1) cationized gelatin production, (2) microsphere production and (3) cross-linking of cationized gelatin microspheres. In order to increase the yield of cationized gelatin microspheres, we aimed to improve the second step, i.e., microsphere production.

Cationized gelatin production

PI 9 (10 g) was completely dissolved in 0.1 M phosphate buffer (PBS, 450 mL) containing potassium dihydrogenphosphate and disodium hydrogenphosphate. Ethylenediamine (31.1 mL) and hydrochloric acid were added, and the pH was adjusted to 5.0. EDC (5.35 g) was added to this solution, which was made up to 500 mL with PBS and left for 18 hours. The solution was

Naoto FUKUYAMA or Hidezo MORI, Department of Physiology, Tokai University, Bohseidai, Isehara, Kanagawa 259-1193, Japan Tel: +81-463-931-121 Fax: +81-463-936-684 E-mail: fukuyama@is.icc.u-tokai.ac.jp

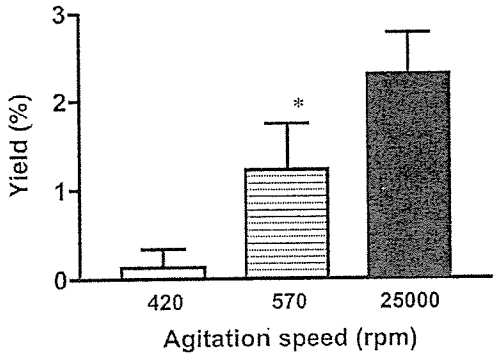

Fig. 1 Yield of ϕ20-32 μm cationized gelatin using a 500 mL three-necked distillation flask.
The open bar shows the control (420 rpm) group, horizontal lined bar, the 570 rpm group and closed bar, the 25,000 rpm group. Data are presented as mean ± SEM. The yield in the 570 rpm group was significantly higher than that in the control group (*p <0.001 vs 420 rpm).

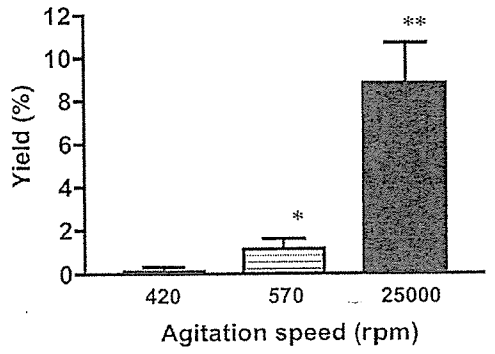

Fig. 2 Yield of ϕ20-32 μm cationized gelatin using a 300 mL three-necked distillation flask.
The open bar shows the 420 rpm group, horizontal lined bar, the 570 rpm group and closed bar, the 25,000 rpm group. Data are presented as mean ± SEM. The yield in the 570 rpm group was significantly higher than that in the 420 rpm group (*p < 0.001 vs 420 rpm). The yield in the 25,000 rpm group was significantly higher than that in the other groups (**p <0.0001 vs other groups).

then dialyzed for 2 days with 16 changes of water. After the dialysis, this solution was freeze-dried for 4 to 7 days to afford cationized gelatin. The conversion rate of carboxyl groups to amino groups was measured by the TNBS method to characterize the product [13].

Microsphere production

In the conventional procedure, cationized gelatin aqueous solution and olive oil were placed in a three-necked distillation flask of 500 mL at 40°C, and centrifuged at 420 rpm for 10 minutes. This solution was stirred for 30 minutes at 0°C. Acetone was added, and the mixture was centrifuged. After centrifugation, the oil layer was removed, and acetone was added. This solution was centrifuged again, homogenized and sieved with ϕ20 μm, ϕ32 μm and ϕ90 μm sieves (Test sieves, #JIS Z 8801, Tokyo Screen Co., Ltd., Japan). The microspheres was dried in a refrigerator overnight, and the yield of each fraction was determined.

In this experiment, we examined the effect of increasing the agitation speed to 570 rpm and 25000 rpm, and the effect of using a smaller three-necked distillation flask (300 mL) to obtain smoother mixing.

Cross-linking of cationized gelatin microspheres

Acetone and hydrochloric acid (7:3) were added to cationized gelatin microspheres, the crosslinking agent GA was added, and the reaction was allowed to proceed for 24 hours. After the reaction, centrifugation was performed and the supernatant was removed. Glycine solution (100 mM) was added to remove GA for one hour. After centrifugation, the supernatant was removed and cross-linked microspheres were cooled with liquid nitrogen, freeze-dried, and weighed.

Gene introduction with the newly developed cationized gelatin microspheres

Gene gelatin complex was prepared by mixing 2 mg of cationized gelatin and 50 μg/100 μl gene (GFP or luciferase). The complex was incubated with rat peritoneal macrophages for 14 days. Effective gene introduction was demonstrated by cellular expression of GFP or luciferase.

RESULTS

Effect of agitation conditions on yield of cationized gelatin

In the conventional method (500 mL/420 rpm), the yield of the ϕ20-32 μm cationized gelatin was 0.13 ± 0.02%, but when the agitation speed was increased to 570 rpm, the yield rose to 1.22 ± 0.52% (*p < 0.001 vs 420 rpm). The yield was further increased to 2.30 ± 0.47% by increasing the agitation speed to 25000 rpm from 570 rpm, but this further increase was not statistically significant (p=0.136)(Fig. 1). Next we used a smaller (300 mL) three-necked distillation flask with agitation at 420 rpm, 570 rpm and 25,000 rpm. When the agitation speed was increased to 570 rpm, the yield rose to 1.12 ± 0.49% from 0.11 ± 0.01% (*p <0.001 vs 420 rpm). The yield was markedly increased to 8.80 ± 1.90% by increasing the agitation speed to 25,000 rpm from 570 rpm (**p <0.0001 vs 420 or 570 rpm) (Fig. 2).

The yields of different-sized microsphere fractions are summarized in Table 1. The use of the highest agitation speed and the smaller flask allowed us to obtain cationized gelatin microspheres of less than ϕ20 μm, which we had not been able to prepare with the conventional method, in addition to increasing the total yield of the cationized gelatin microspheres.

Gene introduction with the new cationized gelatin

We examined the efficiency of the new, smaller-sized cationized microspheres for gene introduction into rat peritoneal macrophages. As shown in Figure 3A, after coincubation of the macrophages and GFP

Table 1 Yields of different-sized cationized gelatines (%).

Flask size (mL) / Agitation speed (rpm)	> ϕ20 μm	ϕ20-32 μm	ϕ32-90 μm	ϕ90 μm >
500/420	0	0.13±0.02	15.1±3.21	14.0±5.30
500/570	0	1.22±0.52*	13.2±3.52	14.1±6.13
500/25000	0	2.30±0.47	17.2±4.10	7.23±1.60
300/420	0	0.11±0.01	19.1±5.32	17.4±7.12
300/570	0	1.12±0.49**	22.1±7.62	11.3±2.52
300/25000	2.12±0.21	8.80±1.90***	32.2±11.0	9.10±2.10

Data are presented as mean ± SEM. *p <0.001 vs 500/420, **p <0.001 vs 300/420
***p <0.0001 vs 300/420 or 300/570

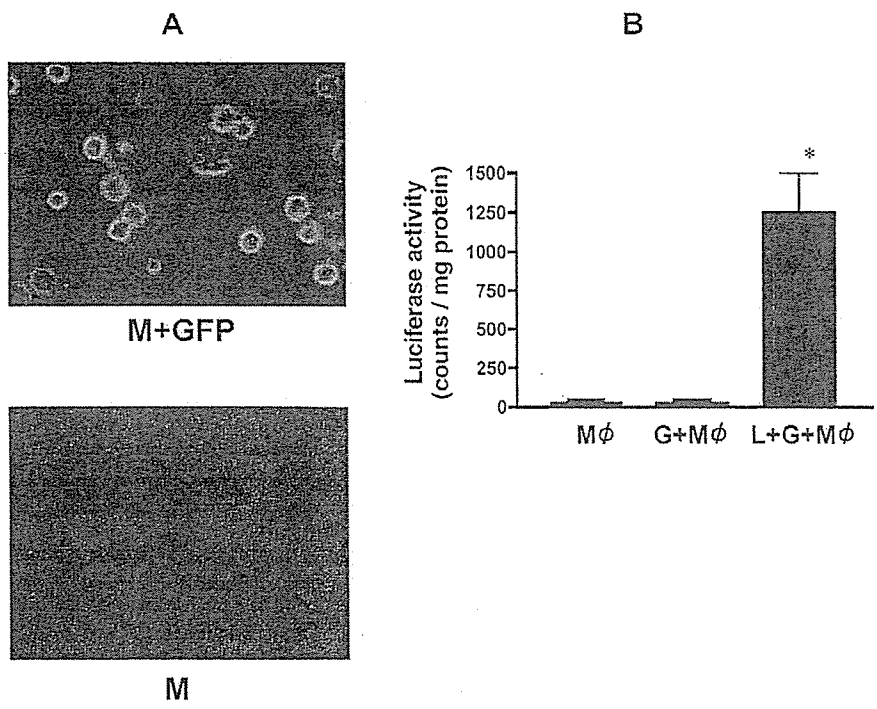

Fig. 3 Gene introduction into rat peritoneal macrophages with cationized gelatin.
A. Upper column: Peritoneal macrophages were coincubated with GFP gene-cationized gelatin complex (M + GFP) for 14 days. GFP was expressed in the cytoplasm of the macrophages. Lower column: Peritoneal macrophages were coincubated with cationized gelatin complex (M) for 14 days. GFP was not expressed in the macrophages.
B. Luciferase activity. Peritoneal macrophages were coincubated with luciferase gene-cationized gelatin complex (L + G + Mϕ, closed bar) or with cationized gelatin (G + Mϕ, horizontal lined bar) or with no additive (Mϕ, open bar) for 14 days. Data are presented as mean ± SEM. The luciferase activity of L+G+Mϕ was significantly higher than that of Mϕ or G+Mϕ (*p <0.01).

gene-cationized gelatin complex, the cells expressed GFP. Coincubation of the macrophages and cationized gelatin alone did not result in expression of GFP. As shown in Figure 3B, after coincubation of the macrophages and luciferase gene-cationized gelatin complex, the cells expressed luciferase activity of 1251 ± 257 (counts/mg protein) on day 14, while the activity in the control group, in which macrophages were cultured alone, was only 5 ± 2 (counts/mg protein) (*p <0.01). The luciferase activity was 8 ± 2 (count/mg protein) in the macrophage + cationized gelatin group.

DISCUSSION

In this study, we showed that the yield of cationized gelatin microspheres of ϕ20-32 μm increased with increasing agitation speed and with the use of a smaller three-necked flask for the agitation of cationized gelatin with olive oil. In addition, cationized gelatin microspheres smaller than ϕ20 μm could be prepared for the first time with the highest agitation speed and the smaller flask.

In the conventional method, 30% of cationized

gelatin finally formed microspheres, but almost all were larger than ϕ32 μm [9]. Gene introduction with cationized gelatin microspheres involves cellular phagocytic activity, which is inefficient for particles as large as ϕ30 μm [6]. By using a speed as high as 25,000 rpm and a smaller flask (300 mL), we were able to increase the yield of cationized gelatin microspheres of ϕ20-32 μm to 8.80%. Furthermore, we could manufacture cationized gelatin microspheres smaller than ϕ20 μm, which could not be obtained by the conventional method, in a yield of 2.12%.

Gedanken *et al.* succeeded in the production of nanoparticles from various chemicals by using ultrasonic irradiation [10]. However, when we used an ultrasonic homogenizer for agitating cationized gelatin and olive oil, the yield decreased to 1.30% .

We previously showed that our gelatin microsphere-gene complexes were introduced into cells by phagocytosis. Since the efficiency of cellular phagocytotic activity is greater for smaller particles, the development of smaller-sized cationized gelatin microspheres is expected to increase the efficiency of gene introduction via phagocytosis. Further, Kaul *et al.* showed that gene introduction into fibroblasts, which exhibit endocytosis but not phagocytosis, was possible by using nanoparticles of polyethylene glycol [11]. Therefore, if our method can be extended to obtain cationized gelatin microspheres in the nano size range, the variety of cells to which they would be applicable may be considerably extended. It is still the case that a gene introduction method with adequate safety and efficiency for clinical application is not yet available [12]. The ingredient, gelatin, used in this study is already in clinical use, and is considered to be safe. Cationized gelatin microspheres cannot be used to introduce genes into all types of cells, and the efficiency of gene introduction is lower than that of viral vectors. However, the use of cationized gelatin microspheres to introduce a gene into endothelial progenitor cells did have an apparent and prolonged therapeutic effect [5, 6]. The smaller cationized gelatin microspheres developed in this study may provide increased efficiency of gene introduction into various cells.

In conclusion, we have improved the preparation of cationized gelatin microspheres for gene transduction, obtaining a greater yield, as well as smaller microspheres, which may have clinical potential.

ACKNOWLEDGEMENT

This work was supported by grants from Tokai University School of Medicine Research Aid in 2004 and 2005, the research and study program of Tokai University Educational System General Research Organization and Kanagawa Nanbyou foundation in 2004, as well as a Grant-in-Aid for Scientific Research in 2003 (No. 15659285) and 2005 (No. 17659375) from the Ministry of Education, Science and Culture, Japan and Health and Labour Sciences Research Grants for Research on Human Genome, Tissue Engineering Food Biotechnology in 2003 (H15-saisei-003). Health and Labour Sciences Research Grants for comprehensive Research on Cardiovascular Diseases in 2004 (H16-jyunkannki(seishuu)-009).

REFERENCES

1) Pfeifer A, Verma IM.: Gene therapy: promises and problems. Annu Rev Genomics Hum Genet 2: 177-211, 2001.
2) Kay MA, Glorioso JC, Naldini L.: Viral vectors for gene therapy: the art of turning infectious agents into vehicles of therapeutics. Nat Med 7: 33-40, 2001.
3) Ferber D.: Gene therapy. Safer and virus-free? Science 294: 1638-42, 2001.
4) Schakowski F, Buttgereit P, Mazur M, Marten A, Schottker B, Gorschluter M, Schmidt-Wolf IG.: Novel non-viral method for transfection of primary leukemia cells and cell lines. Genet Vaccines Ther 2: 1, 2004.
5) Kasahara H, Tanaka E, Fukuyama N, Sato E, Sakamoto H, Tabata Y, Ando K, Iseki H, Shinozaki Y, Kimura K, Kuwabara E, Koide S, Nakazawa H, Mori H.: Biodegradable gelatin hydrogel potentiates the angiogenic effect of fibroblast growth factor 4 plasmid in rabbit hindlimb ischemia. J Am Coll Cardiol 41: 1056-62, 2003.
6) Nagaya N, Kangawa K, Kanda M, Uematsu M, Horio T, Fukuyama N, Hino J, Harada-Shiba M, Okumura H, Tabata Y, Mochizuki N, Chiba Y, Nishioka K, Miyatake K, Asahara T, Hara H, Mori H.: Hybrid cell-gene therapy for pulmonary hypertension based on phagocytosing action of endothelial progenitor cells. Circulation 108: 889-95, 2003.
7) Cascone MG, Lazzeri L, Carmignani C, Zhu Z.: Gelatin nanoparticles produced by a simple W/O emulsion as delivery system for methotrexate. J Mater Sci Mater Med 13: 523-6, 2002.
8) Kittlick PD, Engelmann D.: The glycosaminoglycans in cultures of stimulated rat peritoneal macrophages. 2. Gel chromatographic studies and the behaviour of heparan sulfate. Exp Toxicol Pathol 45: 87-92, 1993.
9) Fukunaka Y, Iwanaga K, Morimoto K, Kakemi M, Tabata Y.: Controlled release of plasmid DNA from cationized gelatin hydrogels based on hydrogel degradation. J Control Release 80: 333-43, 2002.
10) Gedanken A.: Using sonochemistry for the fabrication of nanomaterials. Ultrason Sonochem 11: 47-55, 2004.
11) Kaul G, Amiji M.: Cellular interactions and in vitro DNA transfection studies with poly(ethylene glycol)-modified gelatin nanoparticles. J Pharm Sci 94: 184-198, 2004.
12) Tomanin R, Scarpa M.: Why do we need new gene therapy viral vectors? Characteristics, limitations and future perspectives of viral vector transduction. Curr Gene Ther 4: 357-72, 2004.
13) Rabinovich-Guilatt L, Couvreur P, Lambert G, Goldstein D, Benita S, Dubernet C.: Extensive surface studies help to analyse zeta potential data: the case of cationic emulsions. Chem Phys Lipids 131: 1-13, 2004.

Tokai J Exp Clin Med., Vol. 31, No. 3, pp. 128-132, 2006

Search for appropriate experimental methods to create stable hind-limb ischemia in mouse

Takako GOTO[*1], Naoto FUKUYAMA[*2], Akira AKI[*1], Kazuo KANABUCHI[*1], Koji KIMURA[*1], Hiroyuki TAIRA[*1], Etsuro TANAKA[*3], Noriaki WAKANA[*3], Hidezo MORI[*4] and Hiroshi INOUE[*1]

*Departments of [*1] Surgery and [*2] Physiology, Tokai University School of Medicine*
*[*3] Department of Nutritional Sciences, Tokyo University of Agriculture, Tokyo, Japan*
*[*4] Department of Cardiac Physiology, National Cardiovascular Center Research Institute, Suita, Japan*

(Received June 26, 2006; Accepted July 19, 2006)

Objective: Stable animal models for refractory peripheral arterial disease are not established. A standardized animal model of hind-limb ischemia is required upon searching effective treatment for this condition. The aim of the study is to verify previously used hind-limb ischemia models to find a standard method.
Methods: Using Balb/ca mice six various methods of inducing hind-limb ischemia were applied and two weeks after operation degree of ischemic damage were examined. Six methods include V group, A group, AV group, A-strip group, AV-strip group and Prox-A group (refer the text).
Results: Degree of ischemia was evaluated macroscopically by judging toes, foot, knee, and total hind-limb necrosis. We found that severity of damage was markedly different among different methods. Furthermore the severity of necrosis was not uniform even in the same method group.
Conclusions: The A-strip group in which the femoral artery from the bifurcation of the deep femoral artery to the saphenous artery was stripped appears to be suitable as a stable severe ischemia model. The A group in which the femoral artery were cut just below the bifurcation of the deep femoral artery appears to be suitable as a chronic mild ischemia model.

Key words: angiogenesis, animal model, blood vessels, femoral artery, hind-limb ischemia

INTRODUCTION

Refractory peripheral arterial disease is becoming an important therapeutic target since its incidence has been markedly increasing due to the increase in aged population and patients with diabetes mellitus. Consequently various therapeutic approaches including angiogenic treatment with growth factors or cell transplantation have been attempted using mouse hind-limb ischemia models [1-4]. Scrutinizing these studies we found that experimental methods to create hind-limb ischemia are not standardized. Method of occluding artery varies from ligation, or cutting, to excision of the artery. The targeted artery varies also from the iliac artery [1], the femoral artery [2-4], or the femoral with saphenous artery [5-9]. In some cases, both the femoral artery and vein were occluded. Strangling of the thigh itself was attempted in some studies [10, 11]. As the severity of ischemic damage cannot be uniform in different experimental methods, the comparison of effect among various therapies becomes very difficult.

Another important problem in previously used animal models is lack of data on blood flow when hind-limb is lost. In case of severe ischemic damage in mouse necrosis and loss of hind-limb often occur within three days but in patients of peripheral artery disease ischemia is chronic and acute necrosis is seldom seen. In these patients the improvement of blood flow is one of the key indices in determining effective treatments. Therefore it is mandatory to have an animal model in which chronic hind-limb ischemia is present but necrosis seldom occurs and sequential evaluation of blood flows is possible in order to evaluate various therapies.

In the present study, firstly we examined six methods for inducing hind-limb ischemia in Balb/ca mice and evaluated the severity of ischemic change to search for a stable severe ischemia model. Secondly we selected three methods with mild ischemic changes among six methods which do not produce severe necrosis and examined degree of ischemia by measuring CPK release, muscle weight, and histological changes to find an appropriate mild ischemia model.

MATERIALS AND METHODS

Animals

Seventy-five male Balb/ca mice (12 weeks old, 20 to 30 g, Japan Clea Inc, Ishibe) were used. All operations and measurements were performed under general anesthesia (1.0 to 1.5% isoflurane, 60% dinitrous monoxide, and 40% oxygen). The operation was performed, by only one investigator (T.G.), under a microscope (Konan Operation Microscope 707, Konan Keeler Co. LTD, Japan). To create ischemia, the vessels were cut or resected after ligation of the stumps with sterilized 6-0 silk suture (Azwel Inc, Osaka). The investigation conforms with The Guide for the Care and Use of Laboratory Animals published by the U.S. National Institutes of Health (NIH Publication No. 85-23, revised 1996).

Takako GOTO, Department of Surgery, Tokai University School of Medicine, Isehara, Kanagawa 259-1193, Japan Tel: 0463-93-1121 ext:2280 Fax: 0463-95-7567
E-mail: gotoh-ta@is.icc.u-tokai.ac.jp

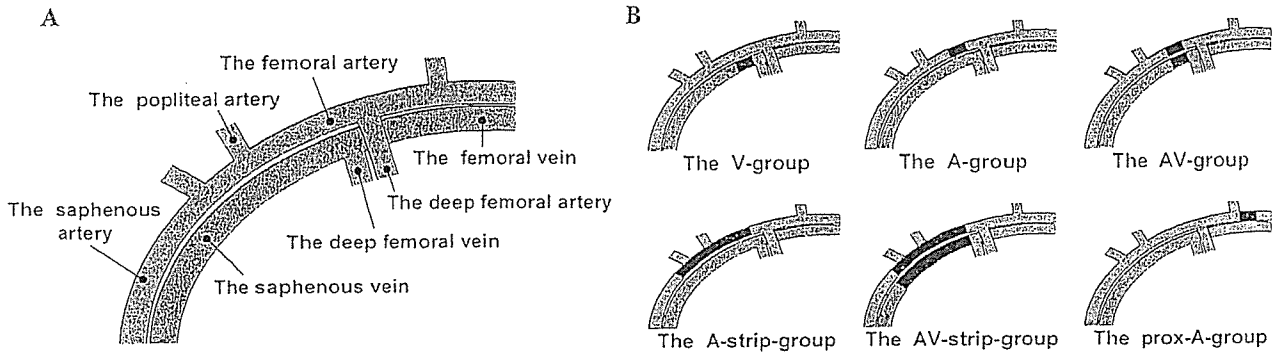

Fig. 1 (A) Schematic illustration of vascular anatomy in the mouse lower limb. (B) Schematic illustrations of surgical procedures in the six groups. The black bar indicates the cut or stripped sites of the vessels.

EXPERIMENTAL PROTOCOLS

1. The six hind limb ischemia models (n = 60)

The following six types of ischemia were created in the right lower limbs of 60 mice (schematic illustrations are presented in Fig. 1). These included, (1) cutting the femoral vein at the distal site of the bifurcation of the deep femoral vein (V-group, n = 10), (2) cutting the femoral artery just below the bifurcation of the deep femoral artery (A-group, n = 10), (3) cutting both the femoral artery and vein (AV-group, n = 10), (4) resection of the femoral artery from the distal site of the bifurcation of the deep femoral artery to the saphenous artery (A-strip-group, n = 10). By disecting the femoral artery as was shown in the Fig. 1B, branches including the popliteal artery were also obstracted and retrograde flows from these branches were completely avoidable. (5) resecting both the femoral artery and vein from the distal site of the bifurcation of the deep femoral artery to the saphenous artery (AV-strip-group, n = 10), and (6) cutting the femoral artery at the proximal site of the bifurcation of the deep femoral artery (Prox-A-group, n = 10).

2. Macroscopic evaluation of ischemic severity

Two weeks after the operation, the ischemic limb was macroscopically evaluated by using graded morphological scales for necrotic area; grade 0: absence of necrosis, grade I: necrosis limiting to toes (toes loss), grade II: necrosis extending to a dorsum pedis (foot loss), grade III: necrosis extending to a crus (knee loss), grade IV: necrosis extending to a thigh (total hind-limb loss).

3. Blood flow measurement

Calf blood flows on both sides were measured below a patella with a noncontact laser Doppler flowmeter (FLO-N1, Omegawave Corporation, Tokyo) before the operation, just after the operation, and two weeks post operatively, and were expressed as the ratio of the flow in the ischemic limb to that in the normal limb.

4. CPK release, muscle weights and histological evaluation in three mild ischemia groups

In additional mice of V-, A-, and AV-groups (n = 5 each) blood samples were obtained from the orbital plexus before the operation and 1, 2, and 7 days thereafter and concentrations of creatine phosphokinase (CPK) were measured. At two weeks after the operation, the animals were sacrificed under an overdose of sodium pentobarbital and the anterotibial, gastrocnemius, and soleus muscles were dissected out and weighed. Histological analysis (HE staining) was performed in each muscle [12].

Table 1 Degree of Ischemic Damage in 6 Groups.

Group \ Grade	0	I	II	III	IV
V group	10				
A group	7	3			
AV group	5	5			
A-strip-group	1	9			
AV-strip-group		6	3	1	
Prox-A-group		3			7

0: no change, I: toes necrosis, II: foot necrosis,
III: knee necrosis, IV: total necrosis

RESULTS

1) Severity of ischemic change in the six groups

Two weeks after the operation necrotic changes were macroscopically evaluated (Table 1). In the V-group, no macroscopic change was observed throughout the experimental period. In other 5 groups tissue necrosis appeared at either toes, dorsum pedis, crus or thigh. The position of necrosis was not uniform even in one group. Loss of total hind-limb was observed only in the Prox-A-group (7/10 mice). The order of necrosis severity among groups were Prox-A-group, AV-strip-group, A-strip-group, AV-group and A-group. The necrosis occurred as early as three days after the operation when it happens.

2) Changes in calf blood flow in the six groups

Just after the operation, calf blood flows were decreased to 30-35% of the pre-operative value without significant differences among the six groups except for the V-group (V-group: 98.5 ± 1.7, A-group: 34.1 ± 12.8, AV-group, 34.4 ± 9.9, A-strip-group: 31.4 ± 3.6, AV-strip-group: 32.9 ± 5.0 and Prox-A-group: 31.3 ±

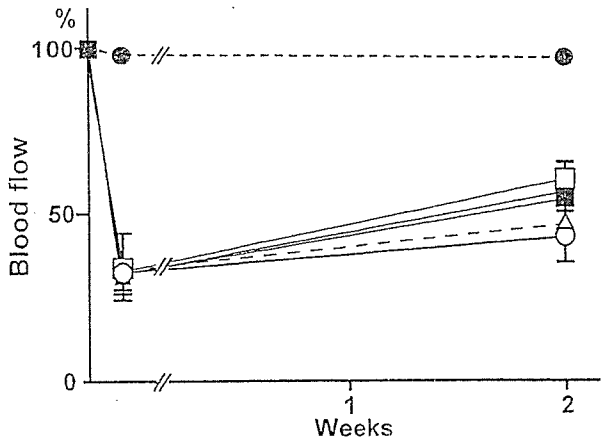

Fig. 2 Blood flow changes in 6 groups. Blood flow is express as a ratio of that in the ischemic limb to that in the opposite limb. V-group: closed circles, A-group: open circles, AV-group: open triangles, A-strip-group: closed triangles, AV-strip group: open squares, Prox-A-group: closed squares. Measurement of blood flows was available only in intact hind-limb or in stable data in case of toes necrosis.

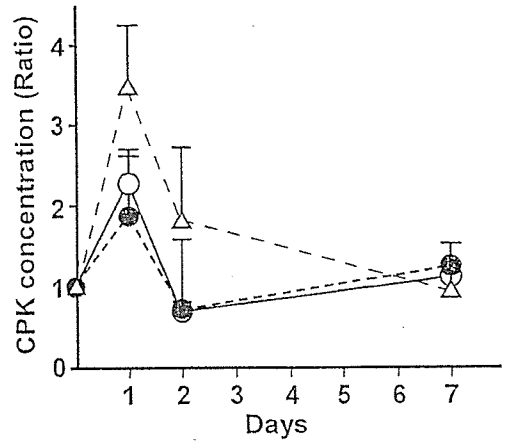

Fig. 3 Concentrations of serum creatine phosphokinase (CPK) in three groups. The concentration is expressed as the value relative to that before the operation. V-group: closed circles, A-group: open circles, AV-group: open triangles.

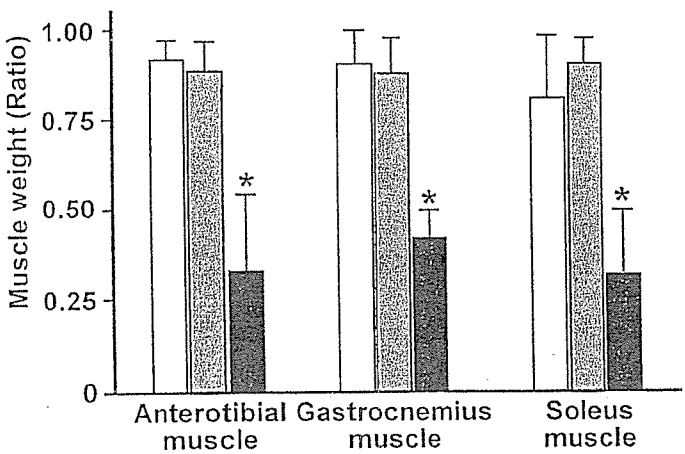

Fig. 4 Muscle weights in the ischemic limb at 14 days after the operation. The weights of the three muscles are expressed as the value relative to those of the same muscles in the opposite limb. V-group: open bar, A-group: grey bar, AV-group: black bar. ($p<0.05$ vs A- and V-groups, ANOVA).

6.5%, respectively, Fig. 2). Two weeks after the operation, calf blood flows had recovered to 45-55% of the pre-operative value (V-group: 97.8 ± 1.2, A-group: 44.7 ± 8.9, AV-group, 48.0 ± 9.0, A-strip-group: 54.0 ± 6.2, AV-strip-group: 57.0 ± 7.3 and Prox-A-group: 59.8 ± 5.1, respectively). The blood flow measurement was applicable only in mice in which calf was well preserved. We found difficulty to obtain stable calf blood flow in some mice with toes necrosis even though their calf was preserved and unstable measurements were omitted. Namely blood flow could be measured in 10 mice in the V group, 10 mice in the A group, 8 mice in the AV-group, 8 mice in the A-strip-group, 7 mice in the AV-strip-group, 3 mice in the Prox-A-group. At two weeks there were no significant differences among the six groups except for the V-group.

3) CPK release, muscle weights and histological evaluation in three mild ischemia groups

As we found that ischemic changes were too severe in A-strips, AV-strip and Prox-A-groups, we selected V-, A- and AV-groups as mild ischemia models. Blood CPK concentrations were significantly elevated one day after the operation in V-, A- and AV-groups ($p<0.05$ vs pre-operation, ANOVA, Fig. 3). Two days after the operation, CPK values had returned to baseline in the A- and V-groups but were still high in the AV-group ($p<0.05$ vs pre-operation, ANOVA). Seven days after the operation, CPK values had returned to baseline in all groups.

Two weeks after the operation, weight loss in the calf muscles was observed only in the AV-group. The values relative to those of the same muscles in the opposite limb were anterotibial: 0.32 ± 0.22, gastrocnemius: 0.42 ± 0.08, and soleus muscles: 0.32 ± 1.8 (Fig. 4). HE staining of the gastrocnemius muscle in the V-group disclosed that there was not obvious changes in the V-group compared with that in the normal limb (Figs. 5A and B). On the other hand, in the A- and AV-groups, microscopic features of necrotic changes such as cell size inhomogeneity, cellular wall degeneration, denucleation, and edema were observed (Figs. 5C

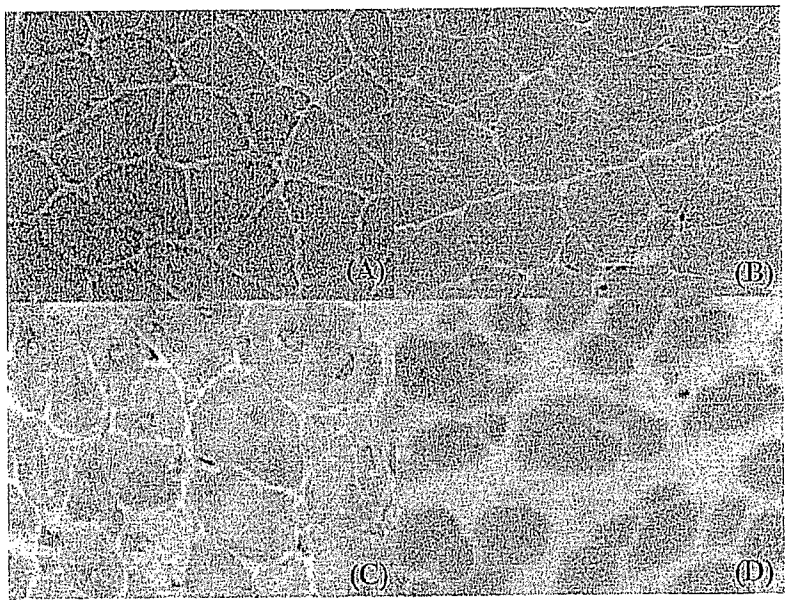

Fig. 5 There was not obvious changes in the V-group compared with that in the normal limb. In the A- and AV-groups, microscopic features of necrotic changes such as cell size inhomogeneity, cellular wall degeneration, denucleation, and edema were observed.

and D). These changes were more severe in the AV-group than in the A-group.

DISCUSSION

The mouse hind-limb has a well-developed innate collateral system and is shown to have remarkably high resistance to ischemia, e.g., a simple ligation of the femoral artery is known to produce no serve ischemic change [1]. This is because the hind-limb would be nourished by collateral circulation via the deep femoral artery and other branches (Fig. 1). As was shown in the Fig. 1A, there are several small branches including the popliteal artery and simple ligation of the femoral artery (A-group) results in obstruction of forward flow, but collateral flows via the deep femoral artery from these branches can retrogradely enter the distal portion of the femoral artery. In contrast, when the site of ligation is proximal, the deep femoral arterial flow will be also interrupted. Similarly in the A-strip group collateral flows from branches cannot enter the distal portion of the femoral artery. When site of ligation is proximal or includes several branches, collateral flow reduces and ischemic change becomes severe. However degree of ischemic damage would not be the same even in the site of ligation because richness and course of collateral vessels differ markedly among individual animals.

As was expected, this study revealed that the degree of ischemic damage varies markedly in six models of mouse hind-limb ischemia. Another important finding of this study is that even in the one model the ischemic damages were not uniform ranging from toes necrosis to knee necrosis as such in the AV-strip-group or from toes necrosis to total hind-limb necrosis in the Prox-A-group (Table 1). Only the A-strip-group showed relatively uniform ischemic damage: 9 toes necrosis and one no change.

On examining effect of various therapies including angiogenic treatments with growth factors or cell transplantation we have to use stable and uniform ischemic damage model, but previous studies used various degree of ischemic damage [1-9]. In this study we showed that A-strip method appears to be most appropriate as a mild ischemia model. The Prox-A method can be utilized when very severe ischemic damage model is necessary.

Regarding mild ischemia model simple ligation of the vein without treatment of the artery (V-group in protocol 2, Fig. 5B) produced only very weak edematous change and this is not an ischemic model. However, obstruction of venous return appears to have additional effects because damage became more serious in the AV-group than that in the A-group (Table 1 and Fig. 5). For example, edematous changes were seen by the histological analysis in the AV-group, and the AV-group showed muscle weight reduction in all anterotibial, gastrocnemius and soleus muscles (Fig. 5). Since venous obstruction is not associated with peripheral arterial disease, pathology under AV-group cannot be consistent with patients suffering from peripheral arterial disease. Although blood flow measurements were possible in both A- and AV-groups, severity of ischemic damage was relatively stable in the A-group, which resembles to the degree of ischemia seen in patients (7 mice showed no necrosis and three had toes necrosis). Taken together, the A-group appears to be the most suitable as a chronic mild ischemia model.

In conclusion, the relatively severe stable ischemia model is created by stripping the femoral artery from the distal site of the bifurcation of the deep femoral artery to the saphenous artery and the mild ischemic model should be made by cutting the femoral artery

just below the bifurcation of the deep femoral artery.

ACKNOWLEDGMENTS

The authors wish to thank Ms. Y Shinozaki for technical assistance. This work was supported by Grants-in-Aid for Scientific Research (15390066, 15659285, 16790761) from the MECSST; The Science Frontier Program of MECSST; Industrial Technology Research Grant Program in '03 from NEDO of Japan; The Research Grants for Cardiovascular Disease (H16C-6), Health and Labour Sciences Research Grants (nano-001, genome-005 and Saisei-003) from the MHLW; the Promotion Fundamental Studies in Health Science of the OPSR, Japan; Tokyo University of Agriculture Soken-Project Research Aid.

REFERENCES

1) Skjeldal S, Grogaard B, Reikeras O, Muller C, Torvik A, and Svindland A. Model for skeletal muscle ischemia in rat hindlimb: evaluation of reperfusion and necrosis. Eur Surg Res 1991; 23: 355-365.
2) Kalka C, Masuda H, Takahashi T, Kalka-Moll WM, Silver M, Kearney M, *et al*: Transplantation of ex vivo expanded endothelial progenitor cells for therapeutic neovascularization. Proc Natl Acad Sci U S A 2000; 97: 3422-3427.
3) Iwaguro H, Yamaguchi J, Kalka C, Murasawa S, Masuda H, Hayashi S, *et al*: Endothelial progenitor cell vascular endothelial growth factor gene transfer for vascular regeneration. Circulation 2002; 105: 732-738.
4) Milia AF, Salis MB, Stacca T, Pinna A, Madeddu P, Trevisani M, *et al*: Protease-activated receptor-2 stimulates angiogenesis and accelerates hemodynamic recovery in a mouse model of hindlimb ischemia. Circ Res 2002; 91: 346-352.
5) Chatterjee BD and Chakraborti CK: Ischaemic mouse thigh model for evaluation of pathogenicity of non- clostridial anaerobes. Indian J Med Res 1989; 89: 36-39.
6) Murohara T, Asahara T, Silver M, Bauters C, Masuda H, Kalka C, *et al*: Nitric oxide synthase modulates angiogenesis in response to tissue ischemia. J Clin Invest 1998;101: 2567-2578.
7) Kanno S, Oda N, Abe M, Saito S, Hori K, Handa Y, *et al*: Establishment of a simple and practical procedure applicable to therapeutic angiogenesis. Circulation 1999; 99: 2682-2687.
8) Rivard A, Silver M, Chen D, Kearney M, Magner M, Annex B, *et al*: Rescue of diabetes-related impairment of angiogenesis by intramuscular gene therapy with adeno-VEGF. Am J Pathol 1999; 154: 355-363.
9) Byun J, Heard JM, Huh JE, Park SJ, Jung EA, Jeong JO, *et al*: Efficient expression of the vascular endothelial growth factor gene in vitro and in vivo, using an adeno-associated virus vector. J Mol Cell Cardiol 2001; 33: 295-305.
10) Wiersema AM, Oyen WJ, Dirksen R, Verhofstad AA, Corstens FH, and van der Vliet JA: Early assessment of skeletal muscle damage after ischaemia-reperfusion injury using Tc-99m-glucarate. Cardiovasc Surg 2000: 186-191.
11) Messina LM, Brevetti LS, Chang DS, Paek R, and Sarkar R: Therapeutic angiogenesis for critical limb ischemia: invited commentary. J Control Release 2002; 78: 285-294.
12) Kuwabara E, Furuyama F, Ito K, Tanaka E, Hattan N, Fujikura H, *et al*: Inhomogeneous vasodilatory responses of rat tail arteries to heat stress: evaluation by synchrotron radiation microangiography. Jpn J Physiol 2002; 52: 403-408.
13) Kasahara H, Tanaka E, Fukuyama N, Sato E, Sakamoto H, Tabata Y, *et al*: Biodegradable gelatin hydrogel potentiates the angiogenic effect of fibroblast growth factor 4 plasmid in rabbit hindlimb ischemia. J Am Coll Cardiol 2003; 41: 1056-1062.

Journal of the American College of Cardiology
© 2006 by the American College of Cardiology Foundation
Published by Elsevier Inc.

Vol. 48, No. 1, 2006
ISSN 0735-1097/06/$32.00
doi:10.1016/j.jacc.2006.04.008

PRECLINICAL STUDY

Erythropoietin Enhances Neovascularization of Ischemic Myocardium and Improves Left Ventricular Dysfunction After Myocardial Infarction in Dogs

Akio Hirata, MD,* Tetsuo Minamino, MD, PHD,* Hiroshi Asanuma, MD, PHD,* Masashi Fujita, MD,* Masakatsu Wakeno, MD,† Masafumi Myoishi, MD,† Osamu Tsukamoto, MD,* Ken-ichiro Okada, MD,* Hidekazu Koyama, BS,* Kazuo Komamura, MD, PHD,§ Seiji Takashima, MD, PHD,* Yoshiro Shinozaki, MD,‖ Hidezo Mori, MD, PHD,§ Masamichi Shiraga, MD, PHD,‡ Masafumi Kitakaze, MD, PHD, FACC,§ Masatsugu Hori, MD, PHD, FACC*

Osaka and Kanagawa, Japan

OBJECTIVES We investigated the effects of erythropoietin (EPO) on neovascularization and cardiac function after myocardial infarction (MI).

BACKGROUND Erythropoietin exerts antiapoptotic effects and mobilizes endothelial progenitor cells (EPCs).

METHODS We intravenously administered EPO (1,000 IU/kg) immediately [EPO(0) group], 6 h [EPO(6h) group], or 1 week [EPO(1wk) group] after the permanent ligation of the coronary artery in dogs. Control animals received saline immediately after the ligation.

RESULTS The infarct size 6 h after MI was significantly smaller in the EPO(0) group than in the control group (61.5 ± 6.0% vs. 22.9 ± 2.2%). One week after MI, the circulating CD34-positive mononuclear cell numbers in both the EPO(0) and the EPO(6h) groups were significantly higher than in the control group. In the ischemic region, the capillary density and myocardial blood flow 4 weeks after MI was significantly higher in both the EPO(0) and the EPO(6h) groups than in the control group. Four weeks after MI, left ventricular (LV) ejection fraction in the EPO(6h) (48.6 ± 1.9%) group was significantly higher than that in either the control (41.9 ± 0.9%) or the EPO(1wk) (42.6 ± 1.2%) group but significantly lower than that in the EPO(0) group (56.1 ± 2.3%). The LV end-diastolic pressure 4 weeks after MI in both the EPO(0) and the EPO(6h) groups was significantly lower than either the control or the EPO(1wk) group. Hematologic parameters did not differ among the groups.

CONCLUSIONS In addition to its acute infarct size-limiting effect, EPO enhances neovascularization, likely via EPC mobilization, and improves cardiac dysfunction in the chronic phase, although it has time-window limitations. (J Am Coll Cardiol 2006;48:176–84) © 2006 by the American College of Cardiology Foundation

Erythropoietin (EPO) is a cytokine that promotes proliferation and differentiation of erythroid precursor cells (1) and is widely used for the treatment of anemia in patients with chronic renal failure (2). Erythropoietin can also exert antiapoptotic and radical scavenger effects on nonerythroid cells (3,4). Indeed, we and others showed that an administration of EPO before or shortly after the onset of ischemia

See page 185

reduced myocardial infarct size and improved cardiac function in acute phases (5–8). Another interesting nonerythroid function of EPO is the promotion of endothelial progenitor cell (EPC) mobilization in animals and humans (9–11), which may enhance neovascularization of ischemic areas (12,13). We hypothesized that EPO increases blood supply to ischemic regions through promoting neovascularization and improves cardiac dysfunction after ischemic insult. Thus, the goal of this study was to characterize the effects of EPO on neovascularization and cardiac function after myocardial infarction (MI) in the chronic phase.

METHODS

All procedures were performed in conformity with the Guide for the Care and Use of Laboratory Animals (NIH publication no. 85-23, 1996 revision) and were approved by the Osaka University Committee for Laboratory Animal Use.

Instrumentation. Forty-seven beagle dogs (Kitayama Labes, Yoshiki Farm Gifu, Japan), weighing 8 to 12 kg were used in these experiments. After an intravenous injection of sodium pentobarbital (15 mg/kg), the dogs were intubated and ventilated. General anesthesia was maintained with 0.5% to 2.0% inhaled isoflurane. After baseline echocardiography and hemodynamic assessment, minimal thoracot-

From the Departments of *Cardiovascular Medicine, †Bioregulatory Medicine, and ‡Hematology and Oncology, Osaka University Graduate School of Medicine, Suita, Osaka, Japan; §Cardiovascular Division of Internal Medicine, National Cardiovascular Center, Suita, Osaka, Japan; and the ‖Department of Physiological Science, Tokai University School of Medicine, Isehara, Kanagawa, Japan.

Manuscript received June 14, 2005; revised manuscript received November 10, 2005, accepted November 30, 2005.

Abbreviations and Acronyms

ABP	=	arterial mean blood pressure
Dil-ac-LDL	=	1,1′-dioctadecyl-3,3,3′,3′-tetramethylindocarbocyanine-labeled acetylated low density lipoprotein
EPC	=	endothelial progenitor cell
EPO	=	erythropoietin
HR	=	heart rate
LAD	=	left anterior descending coronary artery
LCX	=	left circumflex coronary artery
LV	=	left ventricle/ventricular
LVEDD	=	left ventricular end-diastolic dimension
LVEDP	=	left ventricular end-diastolic pressure
MBF	=	myocardial blood flow
MI	=	myocardial infarction
MNC	=	mononuclear cell
UEA-I	=	*Ulex europaeus* agglutinin I
VEGF	=	vascular endothelial growth factor

omy was performed, and then the left anterior descending coronary artery (LAD) was ligated just distal to the first diagonal branch. To ensure that all animals included in the data analysis were exposed to a similar extent of ischemia, animals with excessive myocardial collateral blood flow (>15 ml/100 g/min) were excluded from study as previously described (14).

Experimental protocols. ACUTE EFFECTS OF EPO ON MYOCARDIAL INFARCT SIZE. Either a single dose of EPO (1,000 IU/kg; 5 ml) (n = 6) or the same volume of saline (n = 6) was administered intravenously immediately after the LAD ligation. Regional myocardial blood flow (MBF), area at risk, and infarct size at 6 h after the LAD ligation were determined as described previously (Fig. 1) (14). Recombinant human EPO was provided by Chugai Pharmaceutical Co. Ltd. (Tokyo, Japan). Recombinant human EPO is effective for correcting anemia in the beagle dog (15).

EFFECTS OF IMMEDIATE OR DELAYED TREATMENT WITH EPO ON NEOVASCULARIZATION AND CARDIAC FUNCTION. A single dose of EPO (1,000 IU/kg; 5 ml) was administered intravenously immediately [EPO(0) group, n = 8], 6 h [EPO(6h) group, n = 8], or 1 week [EPO(1wk) group, n = 7] after the LAD ligation. Control animals received the same volume of saline (control group, n = 8) immediately after the LAD ligation.

Hematologic parameters. Blood was sampled from a peripheral vein under pentobarbital (15 mg/kg) anesthesia at the time points indicated in Figure 2. Hematologic parameters, including hematocrit, white blood cell count, and platelet count, were measured.

Cytokine measurements. Plasma levels of vascular endothelial growth factor (VEGF) were measured by enzyme-linked immunosorbent assay (R & D Systems, Minneapolis, Minnesota). The detection limit of the assays was 9 pg/ml. The reliability of this assay in dogs has already been reported previously (16).

Quantification of CD34-positive mononuclear cells. The circulating CD34-positive mononuclear cells (CD34+MNCs) were quantified at the time points indicated in Figure 2. In brief, peripheral white blood cells were stained with a phycoerythrin-conjugated anticanine CD34 monoclonal antibody (BD Pharmingen, San Diego, California). Samples were then subjected to a two-dimensional side-scatter-fluorescence dot plot analysis (FACScan, Becton-Dickinson, Tokyo, Japan). After appropriate gating of

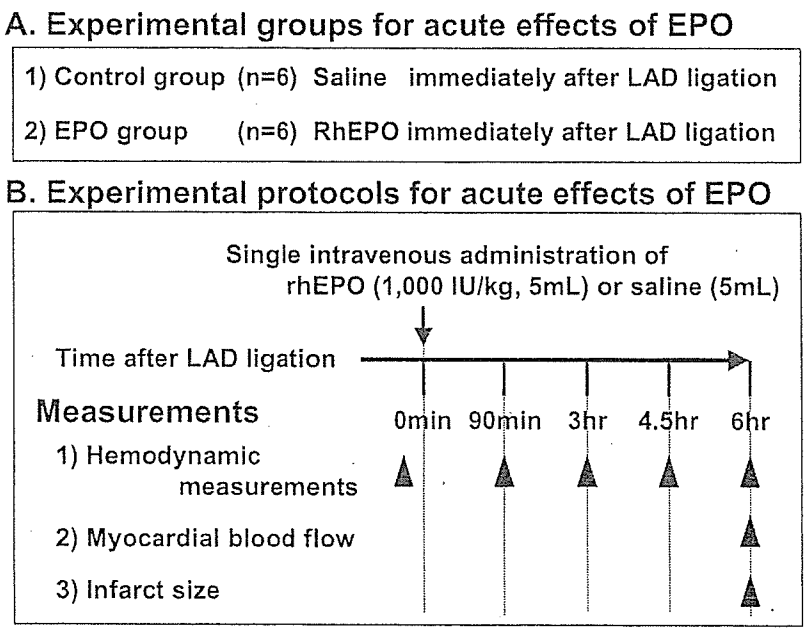

Figure 1. Experimental protocols to investigate acute effects of erythropoietin (EPO) on myocardial infarct size. LAD = left anterior descending coronary artery; RhEPO = recombinant human erythropoietin.

JACC Vol. 48, No. 1, 2006
July 4, 2006:176–84

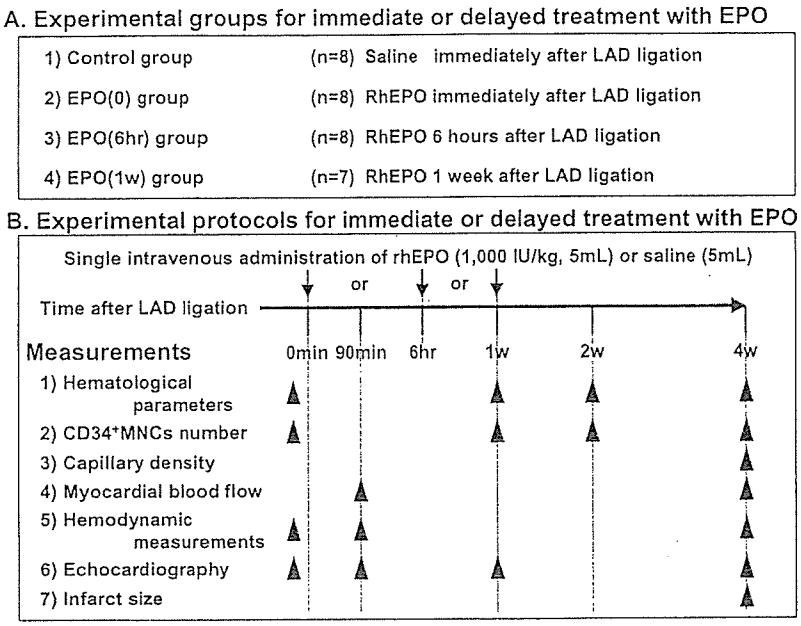

Figure 2. Experimental protocols to investigate effects of immediate or delayed treatment with erythropoietin (EPO) on neovascularization and cardiac function. CD34+MNC = CD34-positive mononuclear cell; other abbreviations as in Figure 1.

MNCs, the number of CD34+MNCs with low cytoplasmic granularity (low sideward scatter) was quantified and expressed as the number of cells per 1-μl blood sample.

In vitro MNC culture assay. Circulating MNCs were isolated from blood (10 ml) of dogs at baseline and 1 week after MI in the control and EPO(0) groups (n = 4 each) by Ficoll density-gradient centrifugation. After MNCs (107 per well) were plated in Medium 199 (Gibco, Grand Island, New York) supplemented with 20% fetal calf serum and antibiotics on human fibronectin-coated six-well dishes. After 7 days in culture, adherent cells were stained for the uptake of 1,1′-dioctadecyl-3,3,3′,3′-tetramethylindocarbocyanine-labeled acetylated low-density lipoprotein (DiI-ac-LDL) (Biomedical Technologies, Stoughton, Massachusetts) and the binding of fluorescein isothiocyanate-labeled *Ulex europaeus* agglutinin I (UEA-I) (Vector Laboratories, Peterborough, England). Double-staining cells were quantified by examining five random microscopic fields (×200 power) (10,11).

Histologic assessments. Four weeks after MI, myocardial tissue was sampled from both ischemic (LAD) and nonischemic (left circumflex coronary artery [LCX]) regions in each group. The tissues in the ischemic region were identified as the edge of the region showing necrosis. These samples were then fixed in 10% buffered formalin, embedded in paraffin, and serially sectioned in the frontal plane at 5-μm thickness. Endothelial cells were immunohistologically stained using rabbit antihuman von Willebrand factor antibody (Dako, Kyoto, Japan) and the Envision+/HRP Kit (Dako) (17). The peroxidase was visualized by incubation with 3,3'-diaminobenzidine, followed by incubation with a DAB-enhancing solution (Dako). We counted the numbers of capillaries and cardiomyocytes in 20 random high-power fields (×400 power), and then calculated the average capillary density and capillary-to-myocyte ratio (18).

Measurements of regional MBF. Regional MBF was determined as described previously (19). Nonradioactive microspheres (Sekisui Plastic Co., Tokyo, Japan) made of inert plastic were labeled with bromine or niobium. Microspheres were administered at 90 min and 4 weeks after MI. The MBF in the LAD region was calculated according to the following formula: time flow = (tissue count) × (reference flow)/(reference count), and was expressed in ml/g wet weight/min.

Hemodynamic measurements. Hemodynamic parameters, such as arterial mean blood pressure (ABP), heart rate (HR), and left ventricular end-diastolic pressure (LVEDP), were measured at the time points indicated in Figure 2. A 5-F sidearm sheath (Radifocus, Terumo, Tokyo, Japan) was placed in the right femoral artery for hemodynamic measurements. A 4-F pigtail catheter (Outlook, Terumo) was placed in the LV for measurement of LVEDP and was connected to a pressure transducer (model DX-200, Nihon Kohden, Tokyo, Japan). The ABP and HR were monitored via the 5-F sidearm sheath.

Echocardiography. Cardiac function was assessed by echocardiography (Sonos 5500, S4-probe, 2-4 MHz, Philips, Bothell, Washington) at the time points indicated in Figure 2. Short-axis views were recorded at the level of midpapillary muscles, and two-dimensional and M-mode views were recorded at the same level. Measurements of left ventricular end-diastolic dimension (LVEDD) and LV ejection fraction were obtained from M-mode views. All measurements were made by one observer, who was blinded with respect to the identity of the tracings.

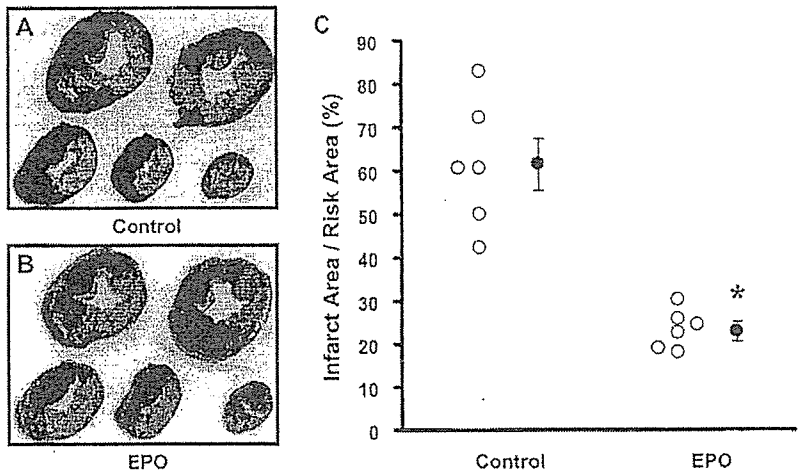

Figure 3. Representative left ventricular cross sections at 6 h after myocardial infarction (MI) in dogs with (B) and without (A) erythropoietin (EPO) treatment. (C) Infarct size at 6 h after MI. *p < 0.05 vs. the control group. **Open circles** = infarct size in each animal.

Infarct size 4 weeks after MI. Myocardial infarct area was determined at the end of the protocol by triphenyltetrazolium chloride staining as described previously (14). Infarct size was expressed as a percentage of the total LV area.

Statistical analysis. Results are expressed as the mean ± standard error of the mean. Comparisons of the time course of the change between groups were performed using two-way repeated measures analysis of variance. Comparisons of other data between groups were performed using one-way factional analysis of variance. If statistical significance was found for a group, a time effect, or a group-by-time interaction, further comparisons were made with paired *t* tests between all possible pairs of four groups at individual time points. The Bonferroni-Holm procedure was used for correction of multiple comparisons. A p value <0.05 was considered to represent statistical significance (20).

RESULTS

Exclusion. Four dogs [acute effects protocol; control: 1, EPO: 0, delayed treatment effects protocol; control: 1, EPO(0): 1, EPO(6h): 0, EPO(1wk): 1] were excluded from analysis because of excessive regional MBF (>15 ml/100 g/min). Thus, 12 and 31 dogs in acute and delayed EPO treatment protocols, respectively, were included.

Acute effects of EPO on infarct size. Myocardial infarct size was significantly smaller in animals receiving EPO compared with those that received saline, but there was no significant difference in regional MBF (9.0 ± 1.0 ml/100 g/min vs. 8.5 ± 1.2 ml/100 g/min) or area at risk (42.9 ± 2.3% vs. 42.3 ± 0.9%) when comparing the two groups (Fig. 3).

Effects of EPO on hematologic parameters. The average change in hematologic parameters was not different when comparing the three EPO-treated groups and the control group over the 4-week experimental protocol (Table 1).

Plasma VEGF levels. Table 2 shows the time course of changes in plasma VEGF level after MI. The plasma VEGF level was significantly and comparably elevated in both control and EPO(0) groups, peaking on 6 h after MI, and returned to baseline at 1 week after MI.

Circulating CD34+MNCs and in vitro cultured MNCs. Figure 4A shows the time course of changes in circulating CD34+MNC number in the different groups. One week after MI, the number of circulating CD34+MNCs increased in all groups. Furthermore, the number of circulating CD34+MNCs at 1 week after MI was higher in the EPO(0) and EPO(6h) groups than in either control or EPO(1wk) group. Two weeks after MI, the number of CD34+MNCs in the control group returned to the baseline. By contrast, the number of CD34+MNCs in the EPO(0) and EPO(6h) groups also decreased but still remained higher than those in either the control or

Table 1. Time Course of Changes in Hematologic Parameters

Parameters	Baseline	1 Week	2 Weeks	4 Weeks
Hematocrit (%)				
Control	52.9 ± 1.7	47.0 ± 1.6	48.9 ± 2.3	53.1 ± 1.8
EPO(0)	52.4 ± 1.1	48.2 ± 1.2	47.9 ± 1.4	53.4 ± 0.7
EPO(6h)	51.5 ± 1.6	49.3 ± 1.6	51.4 ± 1.1	51.3 ± 2.3
EPO(1wk)	48.9 ± 1.0	46.4 ± 1.1	49.4 ± 0.5	50.1 ± 1.0
WBC ($10^3/\mu l$)				
Control	13.8 ± 0.4	15.4 ± 1.4	15.3 ± 0.9	13.5 ± 0.9
EPO(0)	12.6 ± 0.6	14.0 ± 1.1	14.4 ± 0.3	12.3 ± 1.4
EPO(6h)	12.6 ± 0.8	15.6 ± 1.1	13.9 ± 1.0	12.0 ± 0.8
EPO(1wk)	13.1 ± 0.8	14.8 ± 1.2	13.3 ± 0.4	12.9 ± 0.8
Platelet ($10^4/mm^3$)				
Control	27.3 ± 2.0	26.5 ± 1.9	28.4 ± 1.2	26.2 ± 2.0
EPO(0)	28.5 ± 2.0	26.8 ± 4.3	27.0 ± 3.4	28.2 ± 1.8
EPO(6h)	26.9 ± 0.9	27.0 ± 1.4	26.1 ± 1.8	26.1 ± 1.5

Data are presented as mean ± SEM (n = 7 to 8).
EPO = erythropoietin; WBC = white blood cell.

Table 2. Time Course of Changes in Plasma VEGF Levels

Groups	n	Baseline	6 Hours	1 Week	2 Weeks
VEGF (pg/ml)					
Control	4	<9.0	22.5 ± 3.3*	<9.0	<9.0
EPO(0)	4	<9.0	21.6 ± 5.0*	<9.0	<9.0

Data are presented as mean ± SEM. *p < 0.05 vs. baseline.
EPO = erythropoietin; VEGF = vascular endothelial growth factor.

JACC Vol. 48, No. 1, 2006
July 4, 2006:176–84

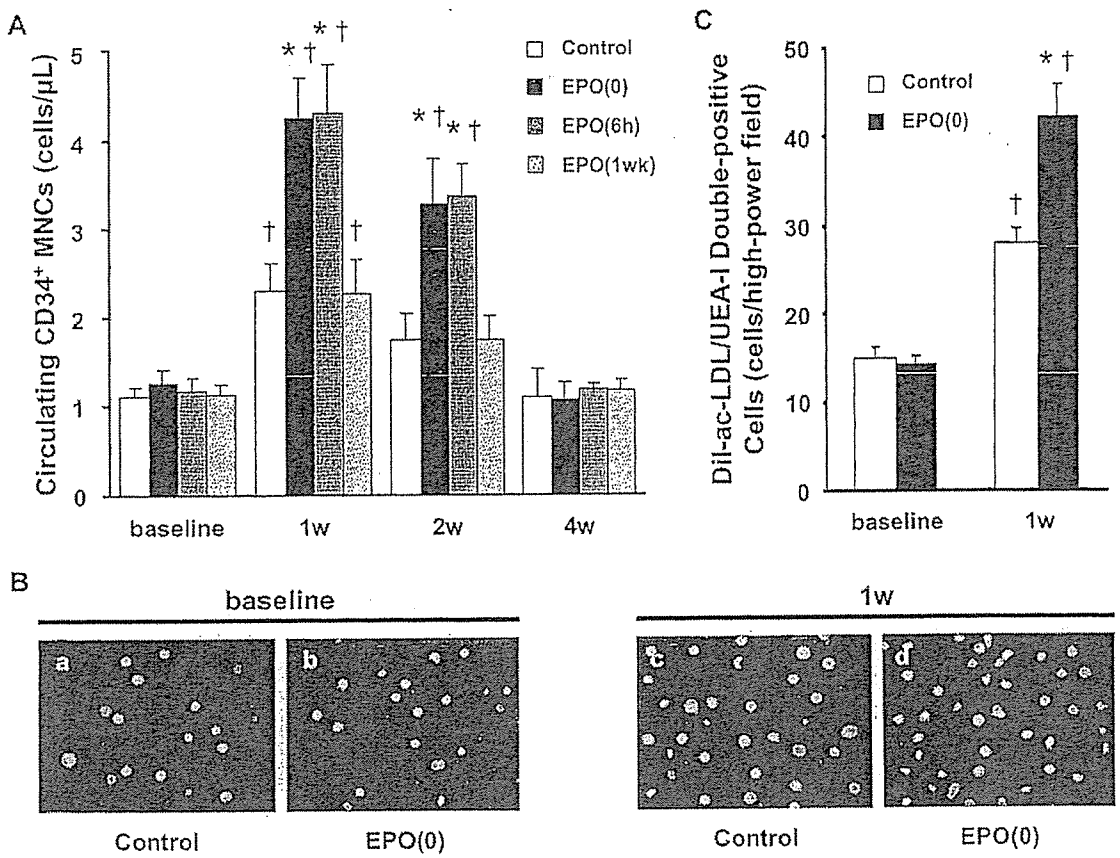

Figure 4. (A) Time course of changes in circulating CD34+MNC count after left anterior descending coronary artery (LAD) ligation in different experimental groups. (B) Representative images of double-stained cultured cells (1,1′-dioctadecyl-3,3,3′,3′-tetramethylindocarbocyanine-labeled acetylated low density lipoprotein [Dil-ac-LDL] and *Ulex europaeus* agglutinin I [UEA-I]) at baseline (a, b) and 1 week after LAD ligation (c, d) from dogs with and without erythropoietin (EPO) treatment immediately after LAD ligation. (C) Quantitative analysis of endothelial progenitor cell culture assay. *$p < 0.05$ vs. the control group. †$p < 0.05$ vs. baseline.

EPO(1wk) group. Furthermore, the administration of EPO 1 week after the LAD ligation did not affect the number of CD34+MNCs at any given time point.

In the culture assay of MNCs, the number of Dil-ac-LDL/UEA-I double-positive cells obtained from blood 1 week after MI increased compared with that at baseline in both control and EPO(0) groups. Importantly, the double-positive cell number obtained from blood 1 week after MI in the EPO(0) group was significantly higher than in the control group (Figs. 4B and 4C).

Capillary density and regional MBF. Figure 5A shows the representative immunohistologic findings in the non-ischemic (panels a to d) and ischemic (panels e to h) regions at 4 weeks after MI. In the nonischemic region, there was no difference in the capillary density and capillary-to-myocyte ratio when comparing groups. In the ischemic region, the capillary-to-myocyte ratio as well as capillary density was significantly higher in the EPO(0) and EPO(6h) groups, but not in the EPO(1wk) group, than in the control group (Figs. 5B to 5C).

Figure 6 shows the changes in regional MBF in the ischemic regions in different experimental groups. There was no significant difference in MBF at 90 min when comparing experimental groups. At 4 weeks after MI, MBF was more increased in the EPO(0) and EPO(6h) groups, but not in the EPO(1wk) group, than in the control group.

Effects of immediate or delayed EPO treatment on cardiac function and infarct size. Throughout the experimental protocols, there was no difference in either ABP or HR when comparing the groups (Table 3).

Figure 7 shows the time course of changes in LVEF (panel A), LVEDD (panel B), and LVEDP (panel C) in different experimental groups. There were no significant differences in baseline LVEF, LVEDD, and LVEDP when comparing the groups.

Ninety minutes, 1 week, and 4 weeks after MI, LVEF was higher in the EPO(0) group than in the other groups. Ninety minutes and 1 week after MI, there was no difference in LVEF when comparing the EPO(6h) group and the control group. When comparing the time points of 1 week and 4 weeks after MI, LVEF decreased in the control and the EPO(1wk) groups but not in the EPO(6h) group. One and 4 weeks after MI, LVEDD was lower in the EPO(0) group than in the other groups. When comparing the time points of 1 week and 4 weeks after MI, LVEDD increased in the control and EPO(1wk) groups but not in the EPO(6h) group. Ninety minutes after MI, LVEDP was lower in the

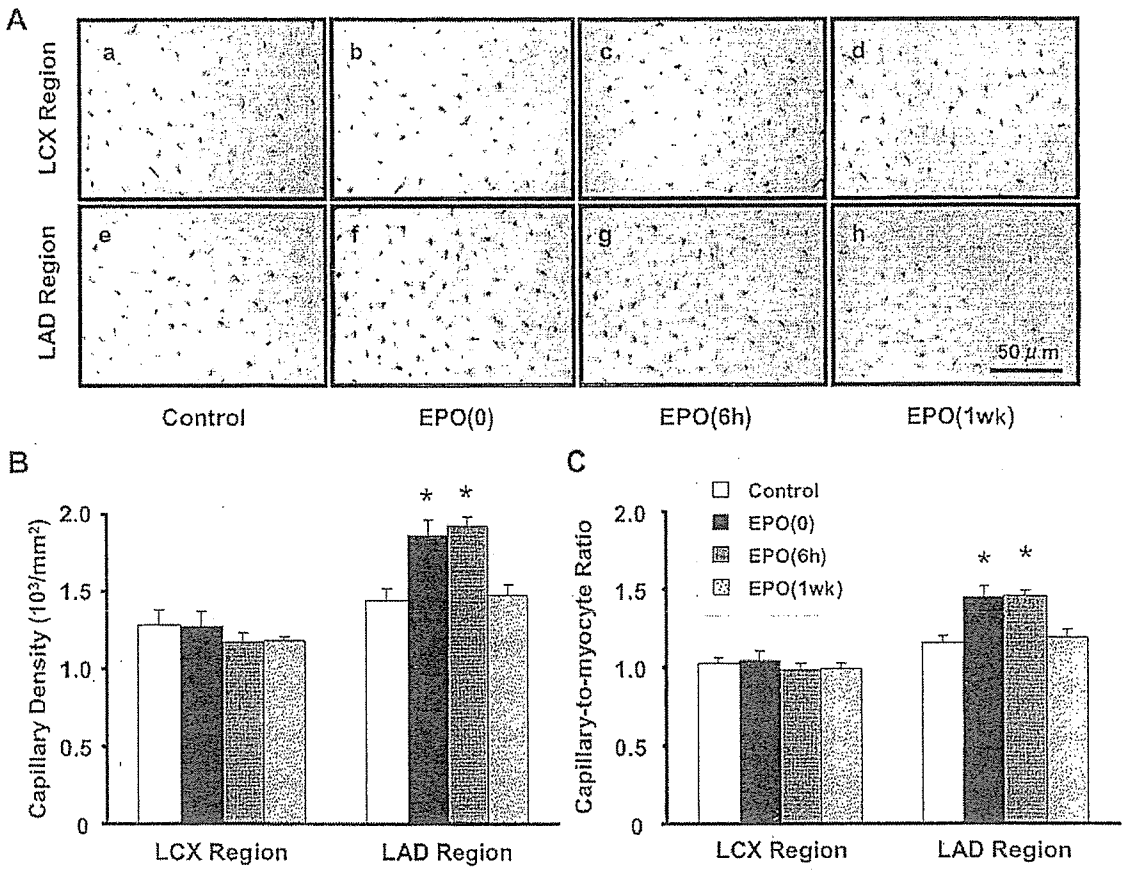

Figure 5. (A) Representative immunohistologic staining with an antibody against von Willebrand factor in nonischemic (left circumflex coronary artery [LCX]) (a, b, c, d) and ischemic (left anterior descending coronary artery [LAD]) (e, f, g, h) regions in different experimental groups. Capillary density (B) and capillary-to-myocyte ratio (C) of nonischemic (LCX) and ischemic (LAD) regions in different experimental groups. *$p < 0.05$ versus the control group. Abbreviations as in Figure 1.

EPO(0) group than in the other groups. Four weeks after MI, LVEDP was lower in the EPO(0) and EPO(6h) groups than in either the control or the EPO(1wk) group.

Myocardial infarct size 4 weeks after MI was smaller in the EPO(0) group than in the control group, although EPO treatment, initiated 6 h and 1 week after MI, did not reduce infarct size (Fig. 7D).

DISCUSSION

The present study showed that EPO administered 6 h after LAD ligation increased circulating CD34+MNCs, capillary density, MBF in the ischemic region, and prevented the worsening of cardiac function without reducing infarct size. The EPO enhances neovascularization, likely via EPC mobilization, and improves cardiac dysfunction in the chronic phase, although EPO has time-window limitations.

We showed that the EPO treatment immediately after the LAD ligation reduced infarct size, which is consistent with observations of previous reports (5–8). Because the infarct size-limiting effects of EPO appear rapidly, the nonerythroid effects of EPO, such as antiapoptosis and radical scavenging (4–8), may contribute to the reduction of infarct size.

Recent reports have shown that circulating CD34+MNC count correlated with EPC number in MNCs culture assay, and both increased at 1 to 2 weeks after EPO administration in animals and humans (9–11). In the culture assay, the number of Dil-ac-LDL/UEA-I double-positive cells obtained from blood at baseline did not differ between the two groups. The number of double-positive cells obtained from blood at 1 week after MI significantly increased compared with that at baseline in the control and EPO(0) groups. Further, the double-positive cell number obtained from blood in the EPO(0) group was higher than in the control group. These findings suggest that EPO augments increases in the number of MNCs that can differentiate into Dil-ac-LDL/UEA-I double-positive cells, an indicator of endothelial cells. Increases in the number of both CD34-positive cells and Dil-ac-LDL/UEA-I double-positive cells strongly suggest that EPO promotes EPC mobilization. The number of CD34+MNCs increased 1 week after MI in the canine model, which is consistent with observations from studies of patients with acute MI (21,22). Furthermore, the number of CD34+MNCs was higher in the EPO(0) and EPO(6h) groups than in the control group. This finding suggests that a single dose of EPO was effective in increasing the number of circulating EPCs after MI. Interestingly,